UNCLASSIFIED

NATIONAL AERONAUTICS AND SPACE ADMINISTRATION

Space Programs Summary 37-44, Vol. II

The Planetary–Interplanetary Program

For the Period January 1 to February 28, 1967

(Title Unclassified)

Classification Changed to
UNCLASSIFIED
JPL-Letter #... NASA-Langley
on Nov. 4, 1970 signed by W.E. Hoare
Date: Jan. 4, 1971 By: R. Barton

GR... 4
Downgra... year
int... declassified
...r 12 years

Copy No. 440

LAB-D01019

...SION LABORATORY
CALIFORNIA INSTITUTE OF TECHNOLOGY
PASADENA, CALIFORNIA

March 31, 1967

CONFIDENTIAL
UNCLASSIFIED

155624

UNCLASSIFIED

SPACE PROGRAMS SUMMARY 37-44, VOL. II

Copyright © 1967
Jet Propulsion Laboratory
California Institute of Technology

Prepared Under Contract No. NAS 7-100
National Aeronautics and Space Administration

ument contains information affecting the national defense of the United States, ... the meaning of the Espionage Laws, Title 18, U.S.C., Sections 793 and 794, the transmis... which in ... unauthorized person is prohibited by law.

GROUP 4 ... vals: declassified ...

UNCLASSIFIED

UNCLASSIFIED

Preface

The Space Programs Summary is a six-volume bimonthly publication designed to report on JPL space exploration programs and related supporting research and advanced development projects. The titles of all volumes of the Space Programs Summary are:

Vol. I. *The Lunar Program* (Confidential)
Vol. II. *The Planetary–Interplanetary Program* (Confidential)
Vol. III. *The Deep Space Network* (Unclassified)
Vol. IV. *Supporting Research and Advanced Development* (Unclassified)
Vol. V. *Supporting Research and Advanced Development* (Confidential)
Vol. VI. *Space Exploration Programs and Space Sciences* (Unclassified)

The Space Programs Summary, Vol. VI, consists of an unclassified digest of appropriate material from Vols. I, II, and III; an original presentation of the JPL quality assurance and reliability efforts, and the environmental- and dynamic-testing facility-development activities; and a reprint of the space science instrumentation studies of Vols. I and II.

Approved by:

W. H. Pickering, *Director*
Jet Propulsion Laboratory

UNCLASSIFIED
CONFIDENTIAL

UNCLASSIFIED

Contents

I. *Mariner IV* Project 1

A. Introduction 1

II. *Mariner* Venus 67 Project 2

A. Introduction 2

B. Systems 3

C. Engineering Mechanics 4

D. Guidance and Control 8

III. *Mariner* Mars 1969 Project 13

A. Introduction 13

B. Engineering Mechanics 14

C. Guidance and Control 22

D. Propulsion 27

References 32

IV. *Voyager* Project 33

A. Introduction 33

B. Engineering Mechanics 34

V. Future Projects 40

A. Introduction 40

B. Some Scientific Instruments for an Unmanned Lunar Orbiter 40

References 43

UNCLASSIFIED

UNCLASSIFIED

I. *Mariner IV* Project

A. Introduction

The *Mariner IV* Project is under the administrative cognizance of the *Mariner* 1967 Project Office, which also directs the *Mariner* Venus 67 Project and the residual activity of the *Mariner* Mars 1964 Project. Residual activity of the *Mariner* Mars 1964 Project consists primarily of continuing analysis of tracking data, publication of results by the principal investigators, and preparation of final reports. However, periodic detection, recording, and commanding activities involving the *Mariner IV* spacecraft have been assigned to the Deep Space Network (DSN). Elements of the experimental facilities at Goldstone Station (DSS 13 and 14) have been used to successfully communicate with the spacecraft. The DSN results will be published periodically in Vol. III of future Space Programs Summaries. *Mariner* Venus 67 Project activities are reported in the following Section II.

The objectives, authorized in December 1965, simultaneously with those for the Venus flight, are:

The primary objective of the Mariner IV Project is to obtain scientific information on the interplanetary environment in a region of space further from the Sun than the orbit of Earth during a period of increasing solar activity in 1967, using the Mariner IV spacecraft still operating in orbit around the Sun.

The secondary objectives are to obtain additional engineering knowledge about the consequences of extended exposure of spacecraft equipment in the interplanetary space environment and to acquire experience in the operation of a planetary spacecraft after a prolonged lifetime in deep space.

During this reporting period, the R&D facilities of the Mars Station (DSS 14) acquired telemetry data (approximately 13.6 hr) on December 28, 1966, and January 15, 1967. Additional telemetry data were obtained in connection with a Class IV solar flare.

UNCLASSIFIED
CONFIDENTIAL

UNCLASSIFIED
CONFIDENTIAL

II. *Mariner* Venus 67 Project

A. Introduction

The *Mariner* Venus 67 Project is under the administrative cognizance of the *Mariner* 1967 Project Office, which is also responsible for the *Mariner* Mars 1964 Project and the *Mariner IV* Project (see Section I).

1. *Mariner* Venus 67 Project

The major task of the *Mariner* 1967 Project is the Venus flyby mission, named the *Mariner* Venus 67 Project. The following mission objectives have been established:

> *The primary objective of the Mariner Venus 67 Project is to conduct a flyby mission to Venus in 1967 in order to obtain scientific information which will complement and extend the results obtained by Mariner II relevant to determining the origin and nature of Venus and its environment.*
>
> *Secondary objectives are to acquire engineering experience in converting and operating a spacecraft designed for flight to Mars into one flown to Venus, and to obtain information on the interplanetary environment during a period of increasing solar activity.*

With the authorizing of this project late in December of 1965, and the launch opportunity occurring in June 1967, the period available to the *Mariner* Venus 67 Project for planning, design, test, and other flight preparation is 18 mo. Because of this minimum length of time, application, to the fullest extent possible, must be made of techniques developed from the experience of prior missions, and existing hardware must be utilized.

The single flight spacecraft, designated M67-2, is currently being prepared by converting the spare spacecraft (MC-4) that was built for the *Mariner* Mars 1964 Project.[1] An *Atlas-Agena D* launch vehicle will inject the spacecraft into a 120-day transit trajectory. The launch readiness date has been set at June 10, 1967, with a 14-day launch period starting June 12. Ranging provisions have been authorized for this mission which will offer the possibility of considerably enhancing the celestial mechanics experiment. At encounter, an unusually sharp perturbation will occur.

[1]Portions of the proof test model (PTM) spacecraft and spares from the MM64 Project are also being prepared as a flight-support spacecraft (M67-1); there will be no PTM as such. The flight-support spacecraft will serve the double function of pseudo-PTM and backup spacecraft for qualifying spare subsystems.

UNCLASSIFIED
CONFIDENTIAL

UNCLASSIFIED

Seven scientific experiments have been approved for the *Mariner* Venus 67 mission:

Experiment	*Principal investigator*
S-band radio occultation	Arvydas J. Kliore, Jet Propulsion Laboratory
Ultraviolet photometer	Charles A. Barth, University of Colorado
Dual-frequency radio propagation	Von R. Eshleman, Stanford University
Helium magnetometer	Edward J. Smith, Jet Propulsion Laboratory
Solar plasma	Herbert S. Bridge, Massachusetts Institute of Technology
Trapped radiation	James A. Van Allen, State University of Iowa
Celestial mechanics	John D. Anderson, Jet Propulsion Laboratory

The first experiment requires the use of only the RF transmission subsystem on the spacecraft, and the last one utilizes only the tracking doppler data received from the RF carrier. Of the remaining five experiments, four are to be accomplished with the existing instrumentation, with only minor modifications. Only the dual-frequency radio propagation experiment of Stanford University requires the incorporation of a new scientific instrument into the payload.

Other changes to the basic spacecraft design are necessitated by the fact that the spacecraft will travel toward, rather than away from, the Sun and also because conversions must be made to accommodate revised encounter sequencing and science payload. In particular, modifications are needed in the following areas:

(1) Scientific data automation system

(2) Antenna pattern and orientation

(3) Thermal control

(4) Solar panel configuration

(5) Planetary sensors

During the January–February reporting period, the spare set of assembled spacecraft equipment successfully completed major qualification testing. Minor rework, magnetic mapping, and final inspection are to be accomplished.

The first system verification test of the flight spacecraft was made with only minor operational problems (of a nontechnical nature) observed; the second system verification test is scheduled for early March. Weight and cg computer runs determined the spacecraft weight to be 540 lb.

All but minor items of mission-related hardware have been delivered to the DSN.

B. Systems

1. Systems-Test-Complex Data System

Support of spacecraft system testing by the systems-test-complex data system (STCDS) continued during this reporting period, and included 250 hr of test support while the M67-1 spacecraft was in the JPL 10-ft Space Simulator. During the continuous 176-hr Phase 1 portion of the test, the STCDS provided telemetry data processing, science data automation system (DAS) data processing (DAS hardline output, and output to Tracks 1 and 2 of the spacecraft tape recorder), and processing of the events and status data channels that had been checked out and were functioning at the time. Data system downtime during this portion of the test was 3.3%, resulting from 39 separate failures, most of which were of a recurrent type and not clearly attributable to either hardware or software, and which were cleared by either restarting or reloading the program. A card reader failure caused 50% of the downtime. During Phase 2 of the simulator test, events and status signals were not available to the STCDS because of removal of all direct-access connections. The data system downtime was 2% during the 82 hr of Phase 2 testing. Twenty-one failures occurred, including many of the same type as encountered previously; however, a memory amplifier card failure was responsible for 50% of the downtime in this period.

Many of the problems which occurred are now understood, and have been remedied by program or software system changes. The Control Data Corp. (CDC) software system monitor program, called Real-Time SCOPE, has been eliminated and replaced by other routines, since it was not well adapted to the input–output functions required by the STCDS application. Remaining problems probably exist during STCDS operation in the remote mode required during spacecraft simulator testing, where

CONFIDENTIAL
UNCLASSIFIED

UNCLASSIFIED
CONFIDENTIAL

the computer is separated by 4000 ft from the data acquisition and display subsystems. These problems can probably be examined and hopefully remedied prior to space simulator tests of the M67-2 spacecraft.

A real-time test support program with increased capabilities was assembled and is being tested during simulated countdown and launch tests of M67-2. A coding freeze will be established after demonstration of acceptable performance in full system test. It is not expected that any additional real-time data processing functions will then be implemented. An improved version of the nonreal-time data processing program has been assembled and checked, and will be developed further to aid in reducing and preparing the recorded spacecraft test data for analysis.

Because of memory core limitations in the CDC 3300 computer, the development of real-time plotting was dropped. Since plotting in nonreal time is an inefficient use of the STCDS, no further development of any plot capability is planned.

The analog modules, and the analog signal amplifiers received in January could not be tested in the STCDS during the spacecraft tests in the simulator because of potential risk to continuous test support. The same constraint was applied to all other hardware and software integration, testing, or assembly. Following initial system testing of the M67-2 spacecraft in mid-February, the analog modules were debugged by the contractor, and operational compatibility with the STCDS was demonstrated. All major items of hardware have now been received and tested in the system.

All except a few events and status channels are now operational as a result of continued testing and debugging of the STCDS/OSE (operational support equipment) interfaces whenever the opportunity occurred.

C. Engineering Mechanics

1. Introduction

This section summarizes the Engineering Mechanics efforts in the thermal area in support of the systems test and operations activities. It also includes descriptions of some of the activities previously completed during the project.

The M67-1 space simulator tests exercised the spacecraft in the space environment and provided valuable information about the thermal behavior of the spacecraft. During the test, additional side shielding had to be added to the spacecraft to raise the average bus temperature approximately 5 deg. The thermal control model (TCM) test had been used to establish the thermal shield configuration. The power estimates used during the TCM tests were approximately 17 w higher than those measured on M67-1.

The test verified that the temperature control subsystem could maintain the spacecraft temperatures within allowable bounds for all combinations of operating mode and flight environment.

The temperature control reference (TCR) has been incorporated into the *Mariner* Venus 67 temperature control subsystem. Design, fabrication and test have been completed. The TCR consists of three assemblies, one mounted on the tip of each of three solar panels. A platinum resistance encapsulated in each assembly measures the equilibrium temperature, from which the absorbed solar thermal energy will be determined. This will be used to compare preflight calculations and solar simulator tests of solar thermal inputs to those experienced in flight. In addition, it will permit determinations of variations of solar absorptance of surfaces with time in space.

When the *Mariner* Venus 67 Project was initiated, a special task group was established to expedite the acquisition and screening of electronic parts. This group was composed of Quality Assurance, Stores, procurement, electronic part specialist, and Parts Acquisition Group personnel.

The major advantages of this approach were:

(1) A single group was responsible for delivering the best quality parts obtainable.

(2) The most knowledgeable personnel were applied to the effort.

(3) Excess parts could be reassigned easily for use by other subsystems.

2. M67-1 Space Simulator Thermal Results

During the period January 13–27, the M67-1 spacecraft underwent system tests in the JPL 10-ft Space Simulator. Two test sequences were performed; a system test (Phase 1) and a thermal test (Phase 2). Phase 1 of the test was intended to exercise the spacecraft system test configuration in a space environment. The thermal test was

UNCLASSIFIED
CONFIDENTIAL

UNCLASSIFIED

accomplished with minimum cables and OSE in order to provide a flight-like thermal configuration.

The test objective for Phase 2 was to verify the ability of the temperature control subsystem to maintain spacecraft temperatures within allowable bounds for all combinations of operating mode and flight environment. Secondary objectives were to check the accuracy of flight temperature transducers, to obtain more accurate flight temperature predictions, and to provide thermal support to the system test team in maintaining safe spacecraft and OSE temperature levels. Significant test results for Phase 2 are given in Table 1.

Table 1. Test data summary (°F)

Bay No.	TCM Earth cruise	M67-1 Earth cruise before change	M67-1 Earth cruise after change	M67-1 postplay-back cruise, after change
I	64	56	62	84
II	48	42	46	69
III	64	55	59	74
IV	61	52	56	76
V	56	50	54	70
VI	64	54	60	79
VII	58	53	61	76
VIII	67.5	64	66.5	82
Bus average	60	53	58	76

The Earth cruise mode shown was for minimum spacecraft power dissipation and lowest solar intensity; the postplayback mode was for maximum power dissipation and highest solar intensity.[1] Results for the Earth cruise mode for the temperature control model (TCM) are given for comparison. M67-1 was initially 7°F cooler than the TCM; the addition of 0.5 ft² of polished aluminum side shields reduced this difference to 2°F. The temperature difference was caused by a high power estimate for use in the TCM test. For the Earth cruise mode, a total of 158 w was dissipated in the TCM bus; the corresponding value measured on M67-1 was 141 w.

All test objectives were met. Satisfactory operation at the coolest and warmest modes has been demonstrated, and adequate margins of safety exist.

[1]Earth cruise: Cavity amplifier, battery charger off, solar intensity = 126 w/ft².

Postplayback cruise: TWT amplifier, battery charger on, gyros on, solar intensity = 290 w/ft².

3. Temperature Control Reference

The purpose of the temperature control reference (TCR) is to compare preflight estimates of solar thermal input (solar intensity × absorptance) to those actually encountered in flight. It will provide a basic comparison between the results obtained with solar simulation and those encountered in space. In addition, it will supply a degree of comparison between laboratory measurement of thermo-optical properties of surfaces and those obtained in space.

To review, the equilibrium heat balance equation for a Sun-dependent item in space can be written:

$$S\alpha A_S + P = \varepsilon A_\varepsilon \sigma T^4$$

where:

S = solar intensity

α = absorptance

ε = emittance

σ = Stefan–Boltzmann constant

A_s = sunlit area

A_ε = emitting area

T = absolute temperature

P = internal power

This is a grossly simplified equation for spacecraft temperature control but serves to illustrate the significance of solar input.

The TCR measures the temperature of a Sun-dependent item for which P (internal power) is zero, and thus, because the geometrics are known, allows the quantity $S\alpha/\varepsilon$ to be computed. For purposes of spacecraft temperature control, the three terms (S, α and ε) are used often. Separate measurements of these terms are subject to sizable uncertainties. While it will be impossible to separate the three quantities from the TCR results, the net product $S\alpha/\varepsilon$ is of significant interest to the spacecraft thermal designer.

The TCR also provides the ability to measure $S\alpha/\varepsilon$ in the solar simulator and compare that measurement to the same quantity in space. This information will aid in reducing the uncertainties in solar simulation thermal testing of future spacecraft.

In addition, the TCR will determine the variation in solar absorptance of painted surfaces with time in space.

CONFIDENTIAL UNCLASSIFIED

UNCLASSIFIED
CONFIDENTIAL

a. Description. As previously mentioned, the TCR consists of three assemblies, one located at the tip of each of three solar panels. (One is not located on the $+y$ panel because of potential interactions with the dual frequency range (DFR) antenna located there.) Each assembly is identical except for the coating used on the sunlit side and the sensor range selection. The three coatings selected are: flat black, and two different types of white coatings.

Physically each TCR (Fig. 1) consists of a 3-in. diameter sensor area, a tee-section fiberglass epoxy laminate support, and an aluminum bracket which attaches to the attitude control gas jet manifold at the tip of the solar panel. A standard flight transducer is mounted on the TCR bracket to measure the temperature of the attitude control manifold.

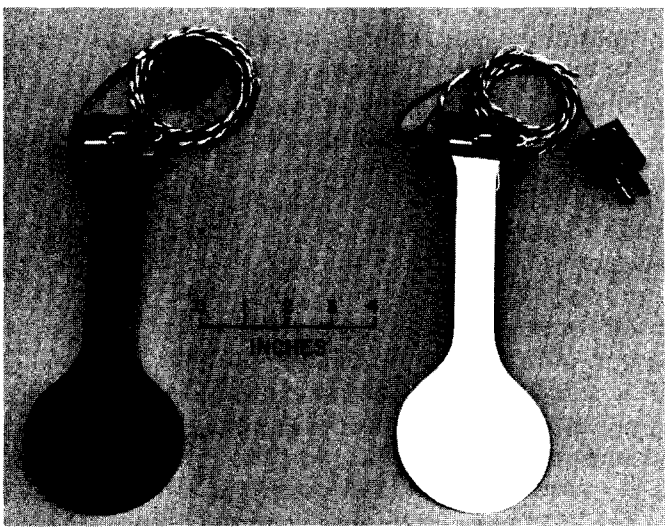

Fig. 1. TCR assemblies

The sensor is encapsulated in the center of the 3-in. diameter area at the outer end. This sensor is a platinum resistance thermometer consisting of three separate coils. The sensors are identical and the coils are used in combinations of series arrangements to provide the proper temperature range for the coatings used. These combinations are shown schematically in Fig. 2.

Spacecraft engineering temperature measurements utilize 500-Ω transducers with appropriate scaling resistors in the data encoder to provide a range of 500–600 Ω, which the encoder can sense.

The TCR sensor resistance values were selected to be compatible with standard data encoder mechanization,

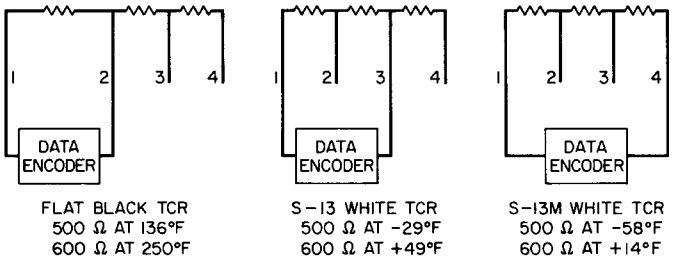

Fig. 2. TCR sensor schematic

but for maximum sensitivity and accuracy the TCR's present the range of 500–600 Ω without scaling resistors to the data encoder.

Encapsulated in the center of the sensor area with the sensor is a 2-in. diameter copper mesh disc to provide temperature uniformity over the center of the sensor area.

The remaining 0.5-in. annulus, having low conductivity and the same coatings, acts as a passive "guard." Similarly, the tee-section support acts as a guard for the sensor leads which are encapsulated therein and which run down to terminals adjacent to the assembly bracket.

b. Thermal performance. Thermally each TCR approximates a thin, flat, infinite plate normal to the Sun, radiating from both sides. The effects of conduction losses and of the thermal gradients through the assembly have been determined analytically and experimentally. Appropriate correction for these effects will be included in final data reduction.

The TCR location at the ends of the solar panels results in negligible radiation coupling to the spacecraft.

Sensor resistance ranges are such that each sensor will be nearly 500 Ω in the vicinity of Earth and increase as the solar intensity increases during the mission. The requirements for data early in the mission and for maximum sensitivity will result in the resistance values exceeding 600 Ω, and thus will be off scale after 105 to 125 days from launch (Fig. 3). Expected changes in absorptance of the white coatings will increase temperature even more rapidly, and the two white units will be off-scale even earlier in the mission.

c. Coating selection. The TCR surfaces are coated to provide engineering information of significance to spacecraft thermal design. The shaded sides of all assemblies are painted black for similar response to simulator back-

UNCLASSIFIED
CONFIDENTIAL

UNCLASSIFIED

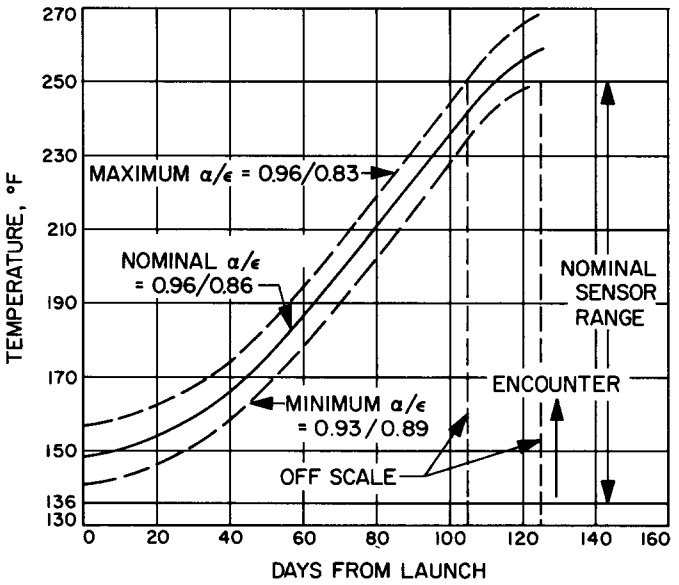

Fig. 3. Typical TCR mission temperature profile (black)

ground radiation and for handling and maintenance simplicity. The coatings selected for the sunlit surfaces are: flat black, S-13 white, and S-13 (modified) white.

The black is Cat-a-Lac[2] flat black epoxy, a widely used spacecraft coating whose properties have been as well established as possible with current radiation measurements technology. Cat-a-Lac was used on, and its space stability verified by, the *Mariner IV* Absorptivity Standard. Results will provide a comparison to space simulator total absorbed energy with that in space, independent of spectral distribution mismatch.

The S-13 white is the best, proven, generally usable engineering spacecraft white paint available at this time and will provide a basis for energy absorption by white surfaces as well as engineering data on the change in absorptance with time in space. S-13 is a zinc oxide pigmented methyl silicone paint. It is used on some continuously sunlit surfaces on the *Mariner* Venus 67 spacecraft.

The S-13 modified is an experimental white paint, similar to S-13 but it is formulated with a treated zinc oxide for improved stability. It is undergoing laboratory development and evaluation at this time and the results will be of engineering interest for future space vehicles.

[2]Finch Paint and Chemical Company, Torrance, California.

4. Electronic Parts Procurement and Screening

At the beginning of the *Mariner* Venus 67 project, a special task group was established to expedite the acquisition of the electronic parts needed for new subsystems and for modifying existing designs.

The task group was organized into four subgroups which provided the controls for the parts procurement, screening procurement, user subsystem interface, and screening vendor monitoring.

The Parts Acquisition Group assigned one individual, the parts representative, to work with the flight subsystem cognizant engineer in specifying the parts requirements. These requirements were reviewed with the parts specialist to verify that the best parts obtainable were being procured to meet the requirements. The parts representative also worked with Quality Assurance, Stores and Receiving to see that the parts were expeditiously delivered for flight subsystem fabrication. The Parts Procurement and Screening Procurement Control team members were responsible for establishing the required procurements, obtaining technical inputs for procurement, and providing status relating to progress for all parts processing activity. The functional monitoring of screening activity was accomplished by screening vendor representatives who were responsible for interfacing with procurement, the electronic parts specialists, Quality Assurance, and Parts Control.

The JPL Electronic Stores maintained financial cognizance of all parts procured and assumed the responsibility of accounting and bonding of the parts through the various stages of processing. All incoming parts from manufacturers were processed through the JPL Receiving and Stores area. Stores prepared the parts for screening, as directed by the parts control personnel.

A semiautomatic status reporting system evolved from a manual system used initially to give faster and more up-to-date information covering the procurement progress and the screening progress. This system is also capable of sorting problem procurements and screening entries from the total status.

Originally a single major screening contract for screening transistors, diodes, resistors, and capacitors was issued. The screening of magnetics was planned to be initiated on a purchase order basis. The concept was modified when it became apparent that a single screening contractor could not instrument and staff adequately to meet the JPL parts and schedule needs. The purchase order method

UNCLASSIFIED

UNCLASSIFIED
CONFIDENTIAL

was established with four additional screening sources. This method proved workable but was slow and consumed more manpower to initiate screening purchase requisitions and followup. JPL Parts Quality Assurance support was used for screening vendor monitoring, screening of urgent and difficult parts, review of vendor screening reports, and acceptance verification of parts supplied for use.

All incoming screened parts were received through stores and placed into stock. The parts delivered for flight use were reviewed and found acceptable by the subsystem cognizant engineer, parts representative, parts specialist and Quality Assurance, prior to release for assembly.

The major advantages of the approach used in the acquisition of parts for *Mariner* Venus 67 were:

(1) A single group was responsible for delivering the best obtainable quality parts for flight applications. This group contained representatives of all other Laboratory disciplines involved in the parts procurement and screening cycle.

(2) Parts procurement efforts in various subsystems were consolidated into one place. Personnel knowledgeable in electronic parts selection, procurement, and screening were efficiently applied to the effort. This has resulted in a more thorough parts acquisition effort.

(3) Late part needs in one subsystem could often be satisfied by using excess parts originally procured for another subsystem.

The largest single disadvantage was the saturation of the available task team resources that occurred during the peak activity periods. This resulted in numerous part delivery delays to the using subsystems.

The *Mariner* Venus 67 task team approach successfully demonstrated, from the parts reliability point of view, the desirability of having one area responsible for obtaining all the electronic parts for the project.

D. Guidance and Control

1. Spacecraft Power

a. Solar cell transducer calibration for use with Mariner Venus 67 and Surveyor. Solar cell transducers similar to those flown on the *Mariner IV* solar panels are being provided for use on each panel of the *Mariner* Venus 67 and *Surveyor* spacecrafts. These transducers consist of three special silicon solar cells which provide engineering measurements of short-circuit current (*Isc*) and open-circuit voltage (*Voc*) for correlation with similar measurements on the total solar panel array. The output of the *Isc–Voc* transducer provides two short-circuit current measurements and one open-circuit voltage measurement. One of the *Isc* measurements is obtained from a cell which has been irradiated to a total flux of 2×10^{14} e/cm^2. This cell is now radiation resistant, and, by comparison with the other *Isc* cell, can provide a quantitative measure of possible radiation damage.

The solar cells used in the *Isc–Voc* transducers are in accordance with JPL Specification 30264A, with the exception of the lower power capabilities of the radiation-resistant cell. The transducers were assembled, using identical materials and similar techniques to those of the respective solar arrays. Each of the cells is covered with a 0.410-μ cutoff filter identical to those used on the solar panels.

b. Calibration. Prior to fabrication each cell was measured in tungsten light at intensities of 100 to 300 mw/cm^2 for *Mariner* and intensities of 100 to 150 mw/cm^2 for *Surveyor*. Temperature measurements from 20 to 150°C were made at each intensity for both the *Mariner* and the *Surveyor* transducers. These laboratory measurements established the temperature coefficient of the individual cells. The tests show that the temperature coefficient is dependent upon intensity and varies approximately 0.2 mv over an intensity range from 100 to 300 mw/cm^2. Each cell also has individual characteristics.

The short-circuit current prediction values are based upon balloon flight-calibrated standard cells, assuming that the short-circuit current is proportional to intensity. The temperature coefficient (ma/°C) for the *Isc* cells also varies as a function of intensity and each cell has its peculiar set of calibration points.

Two transducers of the *Mariner* configuration and two from *Surveyor* were flown at 80,000 ft July 29, 1966, atop a balloon launched near St. Paul, Minnesota. These four transducers, therefore, have calibration data in sunlight at 135 mw/cm^2, and above the major portion of the Earth's atmosphere.

At Table Mountain, all of the flight transducers were calibrated after assembly against balloon flight standard cells. Figs. 4 and 5 show typical flight transducers for the *Mariner* Venus 67 and *Surveyor*, respectively.

UNCLASSIFIED
CONFIDENTIAL

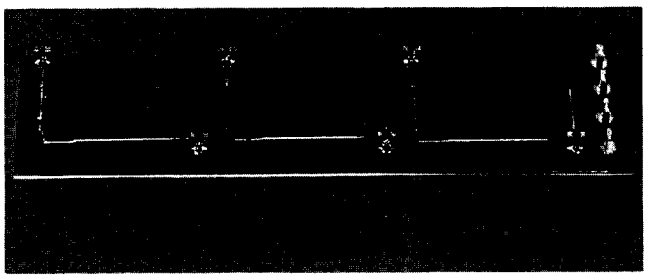

Fig. 4. *Mariner* Venus 67 solar cell transducer

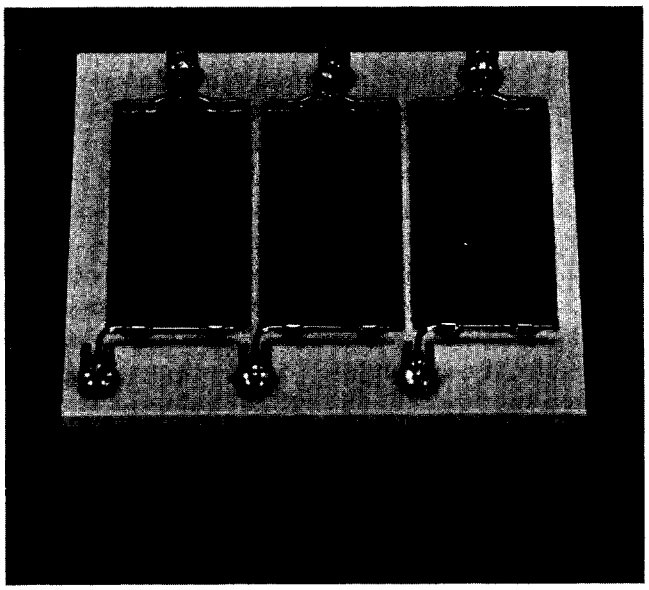

Fig. 5. *Surveyor* solar cell transducer

c. Summary. Data from the *Isc-Voc* transducers will supply information on solar cell and solar panel performance during space environments. These data should prove useful for future solar panel design. A more comprehensive report is now being prepared.

2. Attitude Control Subsystem

Some new problems occurred in the area of the attitude control subsystem during the system testing phase. The chief problem was the failure of the pitch gyro in the gyro control assembly (GCA) to maintain synchronous speed when the GCA was first installed on the M67-2 spacecraft. The GCA was removed from the spacecraft and returned to the Inertial Sensors Group's Gyro Laboratory, and the *Mariner* Mars 1964 PTM GCA was installed on the spacecraft to allow testing to continue. The pitch gyro problem was duplicated in the Gyro Lab, and a decision was made to replace the gyro. The only replacement gyro available was a spare from the *Mariner* Mars 1964 Program and had never been used in a gyro system; it had been tested in January 1966 to confirm its ability for use as a spare, but tests made now, prior to replacement in the GCA, disclosed that it was unusable. Consequently, it was suddenly clear that only one flight-qualified gyro control assembly was available. An immediate time-and-materials contract was placed with the gyro manufacturer, Kearfott Systems Division of General Precision, Inc., for failure analysis of these two gyros, plus another gyro that had previously failed during the *Mariner* Mars 1964 program, and for remanufacture or repair of at least two gyros. The initial duration of the program at Kearfott was 30 days; this entailed working on almost a 168-hr per week basis. Qualification at JPL of the gyro received from the manufacturer at the end of this period would involve an equally intense work load; the goal was to have a flight-qualified GCA back in the M67-2 spacecraft in time for the spacecraft environmental testing, so that the GCA would be considered the flight unit, as the M67-2 spacecraft is considered the flight spacecraft.

The current status of the rework at Kearfott is very satisfactory; although it is difficult to predict the flow of work in such a complicated process as the rebuilding of a miniature floated integrating gyro, this particular rush process seems to be progressing satisfactorily. The failure analysis of the spare gyro has shown that it had a broken pivot; the nature of the break is such that it would have been possible (but improbable) that the pivot was broken before the essentially cursory tests in January 1966. The failure analysis of the original pitch gyro has not yet disclosed the reason for its failure; the failure analysis of the third gyro is not complete. There is no evidence of a general failure trend that would affect all gyros.

Another problem was the apparent loss of torque gain of the jet vane actuators (which act in conjunction with the autopilot to control and orient the thrust vector of the midcourse engine). The rotor of the actuator is a permanent magnet material, Alnico V. The stator consists of a field coil. When current is applied to the field coil, a magnetic field is generated within the actuator; the interaction of this field and the rotor's field causes the rotor to turn. If the output shaft is restricted from turning, a torque is produced which is proportional to the current applied to the field coil. If the shaft is allowed to rotate, mechanical stops at $\pm 27°$ within the actuator restrain the rotor, and the torque produced at the stops acts against the stops.

UNCLASSIFIED

Clearly, the value of torque developed depends on the field strength of the permanent magnet rotor, the current in the stator, and the angle through which the rotor has turned. In a given actuator, the only variable is the field strength of the rotor magnet. The rotor magnet is normally recharged after any operation involving disassembly of the torquer, and the amount of recharge is normally sufficient to magnetically saturate the rotor. The field strength is then adjusted, to obtain the proper torque gain value, by applying a given current to the stator coils. The value of the current applied is determined empirically for a given actuator design; for these actuators, it happens that this current value is approximately equal to the current applied when the autopilot is driven into saturation. This condition occurs during the commanded turns portion of the midcourse maneuver on the spacecraft, but not during the engine firing, since the engine thrust applies a restoring force to the jet vanes.

As a result of the reported loss of torque gain, the procedures for remagnetizing the rotor, adjusting the rotor field strength, and measuring the torque gains were examined closely. Consultation with the designers of the actuators revealed that an essential step in obtaining the proper field strength had never been taken; the step was to force the rotor back to its mechanical null position when current was being applied to the stator. This step ensured that the magnetic field generated by the stator was applied to the rotor full strength, and not decreased by the angle to which the rotor was driven during the procedure. It also was noticed that turning the rotor against the field rapidly effectively turned the torquer into a generator; this action decreased the residual magnetism in the rotor, lowering the torque gain.

The value of torque gain was also found to vary with the direction and angle of measurement; e.g., torques measured in the counterclockwise direction with the rotor at its clockwise stop were higher than torques measured in the clockwise direction at the same stop, for the same applied current. With this new knowledge of the technique and results of adjusting the rotor field strength and measuring the torques, the actuators that were suspected of losing torque gain were remeasured. The results indicated that, since the actuators had not been properly stabilized initially, every time a commanded turn during a simulated maneuver was applied during testing, the actuators were in fact decreasing in rotor field strength and thus in torque gain; however, there was a limit on the decrease, and this limit was within the original torque gain specification on the actuators. Thus, the problem was resolved with no change to the actuators.

The third general problem was the discovery that the Canopus sensor was sensitive to magnetic fields applied perpendicular to the longitudinal axis of the image dissector tube used in the sensor. A conetic cover shields the tube over its surface, with the obvious exception of the photocathode. The construction of the tube is such that three large rings of kovar surround the tube, providing electrical contact with elements of the tube and a metal-to-glass seal for the four sections comprising the outer shell of the tube. Kovar is a permeable metal, and the degaussing fields applied during the type approval degaussing procedure had the effect of shifting the position of the null on the photocathode, which necessitated realigning the optical assembly of the sensor. Since realignment involved invalidating the flight acceptance vibration, an analysis of the field of the undemagnetized sensor, as seen by the helium magnetometer, was undertaken. This analysis showed that the contribution from the sensor was small enough to be acceptable to the magnetometer cognizant engineer, and that, since degaussing reduced the contribution from the sensor at the magnetometer by less than 1 gamma, degaussing was not practical in view of the possible realignment involved. In the future, construction techniques (involving ceramic seals and less segmentation of the tube, if necessary) will be investigated to minimize the problem.

3. Gyro Control Assembly

Two gyro control assemblies (GCAs) for the *Mariner* Venus 67 project exist, S/N 016 (M67-2) the flight unit and S/N 017 (M67-1) the flight spare. Both units are spare *Mariner* Mars 1964 hardware.

Testing was completed on S/N 017 with no anomalies and it was delivered to the Spacecraft Assembly Facility (SAF) August 31, 1966, for integration into the spare spacecraft. While in the spacecraft, this unit was accidentally subjected to input rates which exceeded the handling specification. It was removed from SAF December 13 and tested to verify that no damage had occurred. No significant changes appeared in the data since its initial delivery to SAF. December 16, the GCA was redelivered to SAF for reinstallation into the spacecraft. On January 5, 1967, a problem failure report was generated while in the environmental test area. After vibration the voltage heading readings were 13% off normal. This is a greater error than usual, but considering the conditions in the environmental area is not outside the realm of expected values. No other anomalies have occurred in the GCA performance since its delivery to the spacecraft, and it appears that this unit will remain within all flight specifications. A data summary on this

UNCLASSIFIED

UNCLASSIFIED

unit, compared with *Mariner* Mars data from 1964, is given in Table 2.

Testing was completed on S/N 016 and it was delivered to SAF December 15 for installation into the flight (M67-2) spacecraft. Test results were favorable, comparing closely to those presented for S/N 017. On January 11, while the GCA was installed in the spacecraft at SAF, a problem was reported. Unusually high output voltages were noticed on the pitch channel. Closer investigation showed that this output was varying between 0 and 110 mv at approximately 2 Hz and in phase with a variation in the motor line current. The GCA was then removed from SAF and taken to the Inertial Sensors Laboratory for investigation.

The condition that existed in SAF was not immediately reproduced. It was discovered that when the wheel supply voltage was interrupted for a few hundred milliseconds, the pitch channel output oscillated for approximately 30 sec at approximately 2 Hz, whereas, the roll and yaw channel oscillations died out in less than 1 sec. The gyro was then electrically isolated from the GCA by disconnecting its harness connector. Continued investigation showed that the gyro motor was not running at synchronous speed (400 rps), but at approximately 390 rps. When the wheel voltage was increased from 26 to 28.4 v, the motor pulled into sync. From this and other tests it was concluded that the problem was within the gyro itself and it would have to be replaced. On January 30, S/N 29

Table 2. Gyro control assembly data summary S/N 017

Test	Pitch		Yaw		Roll		Specification
	Mariner Mars 1964	*Mariner* Venus 67	*Mariner* Mars 1964	*Mariner* Venus 67	*Mariner* Mars 1964	*Mariner* Venus 67	
Gyro performance							
KT (°/hr/ma)	133.26	132.26	133.75	133.35	142.15	141.99	138 +5%
RT (°/hr)	−0.092	−0.135	+0.038	+0.036	−0.367	−0.409	±0.5 max after env.
MUS (°/hr/g)	−0.217	−0.203	+0.129	+0.161	+0.222	+0.206	±0.4 max after env.
MUI (°/hr/g)	−0.213	−0.304	−0.054	−0.091	−0.058	−0.125	±0.4 max after env.
Capacitor performance							
I Forward (μa)	1.45	1.84	1.50	1.95	1.48	2.04	5 μa max. with 20 v applied, at the end of 5 min
I Reverse (μa)	2.06	3.13	2.03	3.18	2.11	3.35	
II Forward (μa)	1.62	2.31	1.57	1.93	1.54	2.06	
II Reverse (μa)	2.13	3.33	2.06	2.86	2.06	3.11	
Electronics performance							
gyro loop closing, amps							
Null (mv)	−210	+66	+23	−368	−145	−17	±750 mv dc
+Max. (v)	32.5	31.9	33.0	32.2	32.0	31.5	+30 v dc min
−Max. (v)	34.0	33.9	34.0	33.9	34.0	33.9	−30 v dc min
Gain $\frac{\text{v dc}}{\text{v rms}}$	632	635	632	632	610	609	600 ±50
Command current regulator	*Mariner* Mars 1964		*Mariner* Venus 67				
+Ic (μa)	4.71313		4.69918				+4.6942 ± 0.05 ma
−Ic (μa)	4.72245		4.69204				+4.6942 ± 0.05 ma
Difference (μa)	0.00932		0.00714				−
Roll one-shot							
+T (sec)	12.0		12.1				12.0 ±1.2 sec
−T (sec)	12.6		12.7				12.0 ±1.2 sec
Capacitor cycle							
T (sec)	14.7		14.5				14.0 ±1.5 sec
GCA performance							
command rate							
85°F (°/hr)	620.92	619.61	–	–	664.82	663.39	Nom ±1.5°/hr max
100°F (°/hr)	620.45	618.97	–	–	664.32	662.59	Nom ±1.5°/hr max
115°F (°/hr)	619.86	618.34	–	–	663.84	661.80	648 ±32°/hr (nom)
130°F (°/hr)	619.79	617.64	–	–	663.23	660.96	Nom ±1.5°/hr max

CONFIDENTIAL
UNCLASSIFIED

UNCLASSIFIED
CONFIDENTIAL

gyro was removed from the GCA. Testing was immediately started on S/N 27 gyro, the only qualified replacement unit from the *Mariner* Mars 1964 program. This unit was found to be defective and further tests showed the problem to be a possible broken pivot within the gyro indicating it would have to be torn down for repair. On February 2, gyros S/N 27 and 29, along with 21, a possible repairable unit, were hand-carried to the manufacturer for teardown analysis, repair and rebuild. The goal was to recover two usable gyros from the three available for rework.

The anomaly with S/N 29 motor was not verified at the vendor's facility and the gyro appeared normal. Since a large amount of data was available to show that the problem was within the gyro itself and not in the rest of the GCA, this unit was declared unusable on the assumption that whatever caused the problem once could repeat. A subsequent teardown of the gyro showed general workmanship, external of the gimbal, to be excellent. A teardown of the gimbal and motor assembly indicated nothing that could explain the problem directly. The analysis is not complete at this time, however, and further work will insure that whatever caused the problem could not exist in all units. The teardown of S/N 27 showed, again, excellent workmanship and verified the theory of a broken pivot. The motor and gimbal assembly from this unit was tested and declared usable, and the pivots and jewels were replaced with new items. A motor and gimbal assembly from a group of "off the shelf" similar units was selected, tested, and declared a reliable replacement unit for the S/N 29 gimbal. Both gyros have, to date, been rebuilt to the case and are in similar stages of calibration and test. S/N 21 gyro was not torn down since tests showed that its motor was less desirable as a replacement than either of the two which were finally selected. Delivery of the two rebuilt gyros is expected on or about March 3, 1967. If delivery is accepted March 3, a turnaround time of 29 days will have been accomplished for the analysis, repair, and rebuild of two gyros. This is considered extremely fast work for this task.

A backup plan exists if neither rebuilt gyro will meet the specifications necessary to accept it. A fourth gyro, S/N 18, exists which was rejected from the GCA during the *Mariner* Mars 1964 program. Evidence at that time showed an oscillatory output at, or near, the loop resonant frequency while mounted in the spacecraft. This condition has not been reproduced, and no concrete evidence exists to explain the problem. Tests have been run to prove that the problem was caused by interaction with the loop. The tests were inconclusive, but this still remains as the most likely cause of the problem. As a backup, then, this gyro could be placed in the yaw channel and the yaw gyro transferred to the pitch channel. Tests have been run to verify the feasibility of this plan, and no apparent problems exist. The problem with the gyro has never been completely explained and this unit is somewhat noisier than any of the other units in the systems. Therefore, this plan remains as a backup only.

After receipt of the two gyros from the vendor, S/N 27 will be installed into the GCA if tests are acceptable. An all-out effort will be made to receive this gyro, FA vibration test it in the PTM GCA with a mocked-up spacecraft bay, install it into S/N 016 GCA, and calibrate the system in time for it to be installed into the spacecraft for all system-level FA testing. Present scheduling indicates that this may be possible if work continues around the clock after receipt of the gyro.

UNCLASSIFIED
CONFIDENTIAL

UNCLASSIFIED

III. *Mariner* Mars 1969 Project

A. Introduction

The *Mariner* Mars 1969 Project was initiated in late-December 1965 and formally tasked on February 1, 1966. The primary objective is to conduct two Mars flyby missions in 1969 to make exploratory investigations of the planet which will set the basis for future experiments—particularly those relevant to the search for extraterrestrial life. The secondary objective is to develop the technology needed for succeeding Mars missions.

The spacecraft design concept will be based on the configuration of the successful *Mariner IV* spacecraft, with considerable modifications to meet the 1969 mission requirements and to enhance mission reliability.

The launch vehicle will be the *Atlas/Centaur* SLV-3C. This vehicle, developed under contract for and direction by the Lewis Research Center by General Dynamics/Convair, has a single- or double-burn capability in its second stage and a considerably increased performance rating over the *Atlas D/Agena D* used in the *Mariner IV* mission.

Mariner Mars 1969 missions will be supported by the Eastern Test Range launch facilities at Cape Kennedy, the tracking and data acquisition facilities of the Deep Space Network, and other NASA facilities.

Six planetary-science experiments have been tentatively selected by NASA (subject to integration capability) for the *Mariner* Mars 1969 missions; they are listed in Table 1. Additionally, a planetary-approach-guidance engineering experiment will be incorporated to test the feasibility and flight-readiness of on-board optical sensors and associated data processing techniques necessary for optical approach guidance.

Table 1. *Mariner* Mars 1969 scientific investigations

Experiment	Scientific investigator	Affiliation
Television	R. B. Leighton[a]	California Institute of Technology (CIT)
	B. C. Murray	CIT
	R. P. Sharp	CIT
	N. H. Horowitz	CIT
	J. D. Allen	Jet Propulsion Laboratory (JPL)
	A. G. Herriman	JPL
	L. R. Malling	JPL
	R. K. Sloan	JPL
	N. Davies	Rand Corporation
	C. Leovy	Rand Corporation
Infrared spectrometer	G. C. Pimentel[a]	University of California, Berkeley (UCB)
	K. C. Herr	UCB
Ultraviolet airglow spectrometer	C. A. Barth[a]	University of Colorado
	W. G. Fastie	Johns Hopkins University
Infrared radiometer	G. Neugebauer[a]	CIT
	G. Munch	CIT
	S. C. Chase	Santa Barbara Research Center
S-band occultation	A. J. Kliore[a]	JPL
	D. L. Cain	JPL
	G. S. Levy	JPL
Celestial mechanics	J. D. Anderson[a]	JPL

[a]Principal investigator.

CONFIDENTIAL UNCLASSIFIED

UNCLASSIFIED
CONFIDENTIAL

The launch period available for 1969 Mars launches using planar and dog-leg direct-ascent trajectories runs from the middle of February to the beginning of April. Arrival is planned to occur between August 1 and 10, 1969; two separate aiming points will be chosen.

During this reporting period, the series of subsystem preliminary design reviews was commenced. The structure, infrared spectrometer, flight command, temperature control, CC&S, radio frequency, television, infrared radiometer, flight telemetry, and attitude control subsystem reviews have been conducted. The data storage, mechanical devices, cabling, pyro electronics, power, propulsion, scan control, ultraviolet spectrometer, and data automation subsystems remain to be reviewed in March.

A letter contract was executed with Electro-Optical Systems for pyro electronics design, and a purchase order was sent to Wilorco for spacecraft power simulators (for use in science subsystem testing operations), in January. In February, the following Phase I contracts were executed: power (letter contract) with Electro-Optical Systems; TV optics (letter contract) with Fairchild Camera and Instrument Corporation; propulsion (definitive) with TRW; data automation subsystem (definitive) with Litton Systems; and ultraviolet spectrometer (definitive) with University of Colorado. Preparations continued for the initiation of a number of Phase II efforts.

System design of the spacecraft operational support equipment is under way. A number of configuration and design changes to the flight spacecraft were completed during the period. The spacecraft antennas, described in more detail under Engineering Mechanics, now consist of a conical feed on a taller mast than used in *Mariner* Mars 1964, for the low gain, and a circular parabolic reflector replacing the elliptical reflector of 1964, for the high gain. The telemetry and related subsystems were modified to accommodate three frequency-multiplexed channels and to replace the PN synchronization with bit synchronization carried out on the ground, using the telemetry and command processors at the DSIF stations. A science channel, operated during encounter at 66⅔ bits/sec, and during playback at 270 bits/sec, will contain scientific data; an engineering channel, operated throughout the flight at 8⅓ or 33⅓ bits/sec, will carry engineering telemetry. A block-coded channel, operated at 16.2 kbits/sec, can provide playback or real-time DAS scientific data when the 210-ft advanced antenna system is available during encounter and playback. These changes will be described in detail in a subsequent SPS.

B. Engineering Mechanics

1. Introduction

The scope of the Engineering Mechanics support of the *Mariner* Mars 1969 project has been defined in SPS 37-41, and 37-42, Volume II.

At the spacecraft system level, the current *Mariner* Mars 1969 spacecraft mechanical configuration is presented, together with the description of those changes occurring in the configuration since the last report. Additionally, a description of the temperature control design of the spacecraft system is given.

At the subsystem level, a description of the temperature control subsystem hardware is presented and also a description of the solar panel boost dampers, a part of the mechanical devices subsystem.

A summary of the results of an investigation of various conversion coatings for the corrosion protection of magnesium is also presented.

2. Spacecraft Configuration

Since the last report on the *Mariner* Mars 1969 spacecraft configuration (SPS 37-41, Vol. II), the spacecraft design has undergone considerable change. As of this date, the spacecraft configuration is relatively firm and is shown in Fig. 1.

The salient aspects of this configuration are:

Octagon. The octagonal main electronic compartment is the same size and shape as the *Mariner* Mars 1964 design. The attitude control/CC&S bay has been interchanged with the science bay to provide a more uniform distribution of dissipated power for temperature control purposes. Additionally, several of the bays have been repackaged to provide more efficient utilization of the available volume.

Solar panels. Four identical panels with a total area of 83 ft^2 are attached to the outboard corners of alternate bays of the octagon. During boost the panels are latched to each other through a spring/damper mechanism and a pyrotechnic pinpuller. After release of this latch, the panels are driven to a plane normal to the spacecraft z axis by deployment clock springs at the hinge line and latched to cruise dampers mounted on the outboard face of each solar panel bay.

UNCLASSIFIED
CONFIDENTIAL

Mechanics support of the
been defined in SPS 37-41,

evel, the current *Mariner*
ical configuration is pre-
cription of those changes
since the last report. Addi-
emperature control design
en.

escription of the tempera-
re is presented and also a
oost dampers, a part of the

an investigation of various
rrosion protection of mag-

Mariner Mars 1969 space-
1, Vol. II), the spacecraft
able change. As of this date,
relatively firm and is shown

onfiguration are:

ain electronic compartment
as the *Mariner* Mars 1964
CC&S bay has been inter-
to provide a more uniform
ver for temperature control
al of the bays have been
efficient utilization of the

l panels with a total area of
tboard corners of alternate
oost the panels are latched
g/damper mechanism and a
release of this latch, the
ormal to the spacecraft z axis
at the hinge line and latched
n the outboard face of each

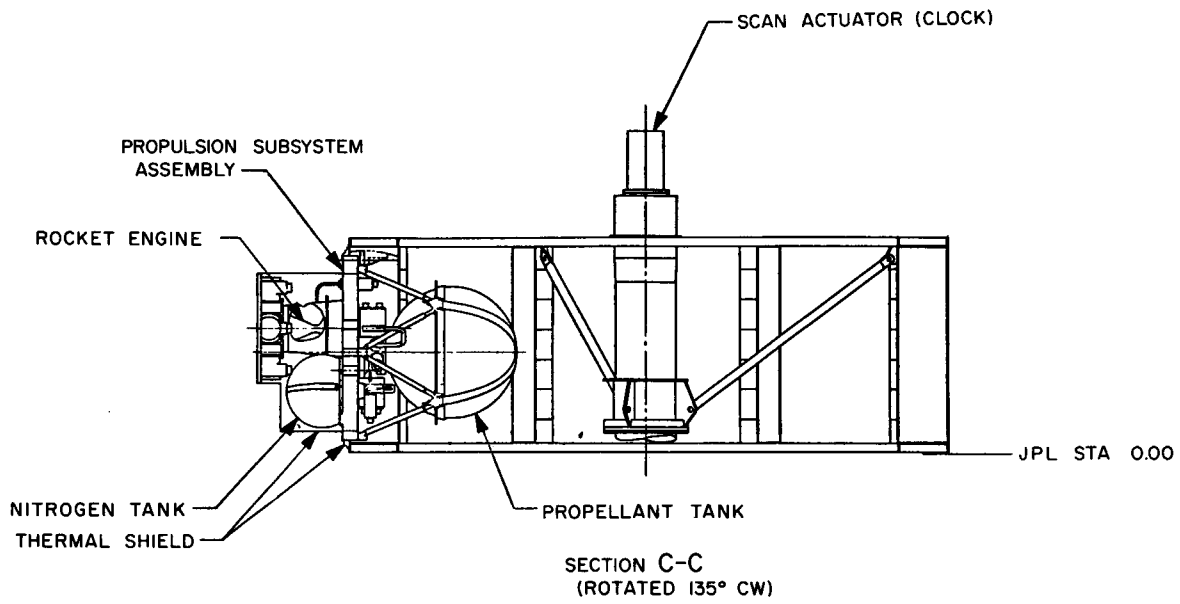

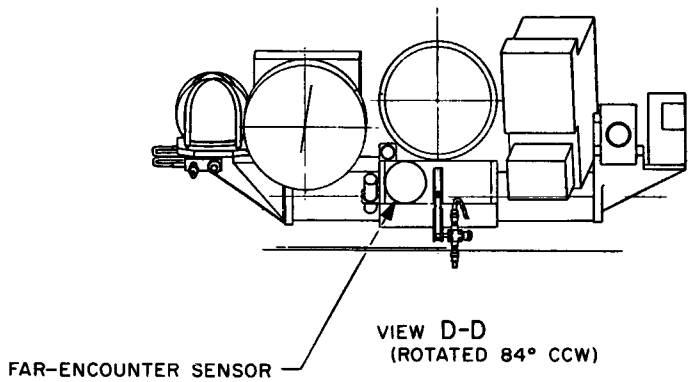

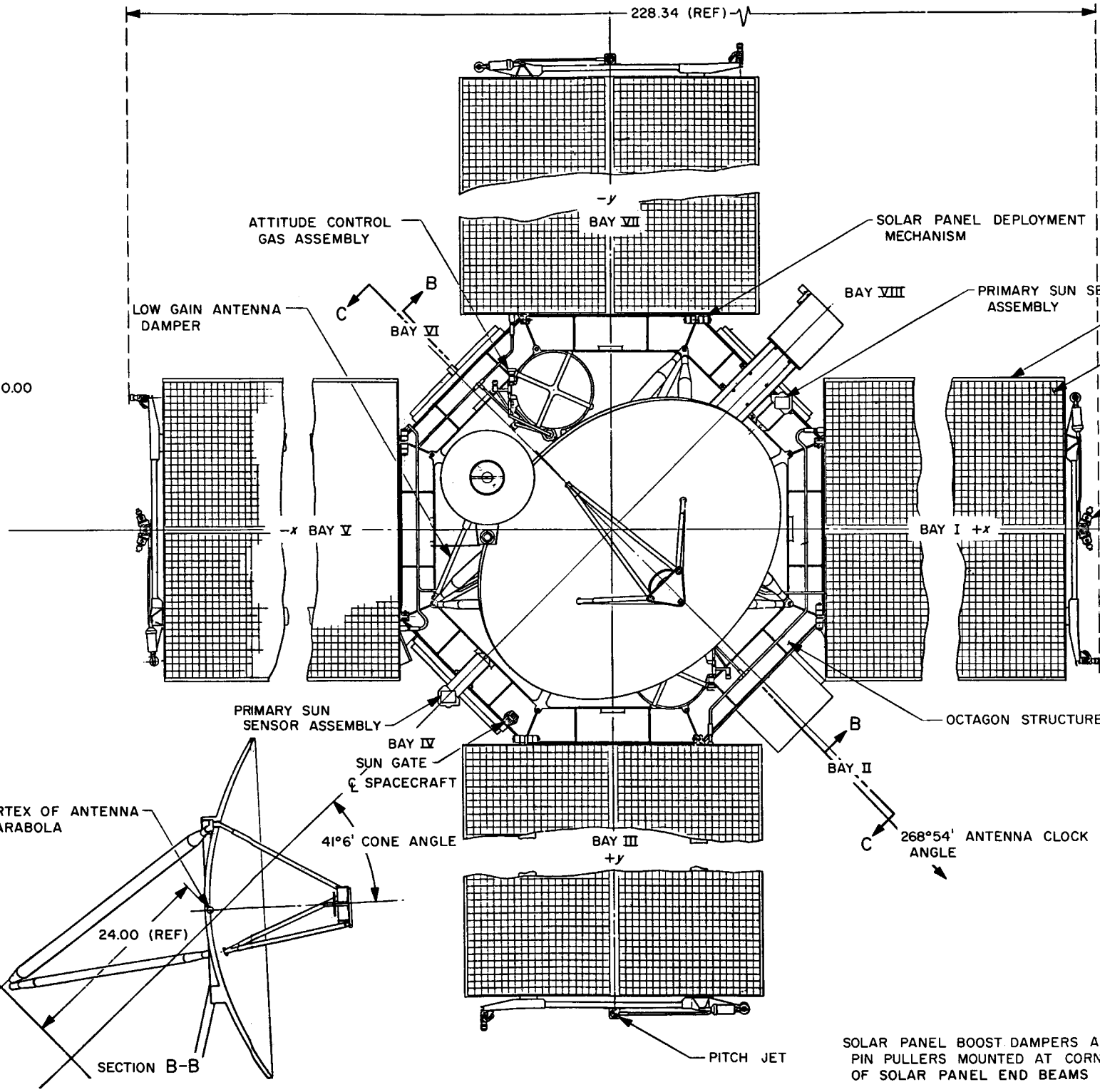

ASSIFIED

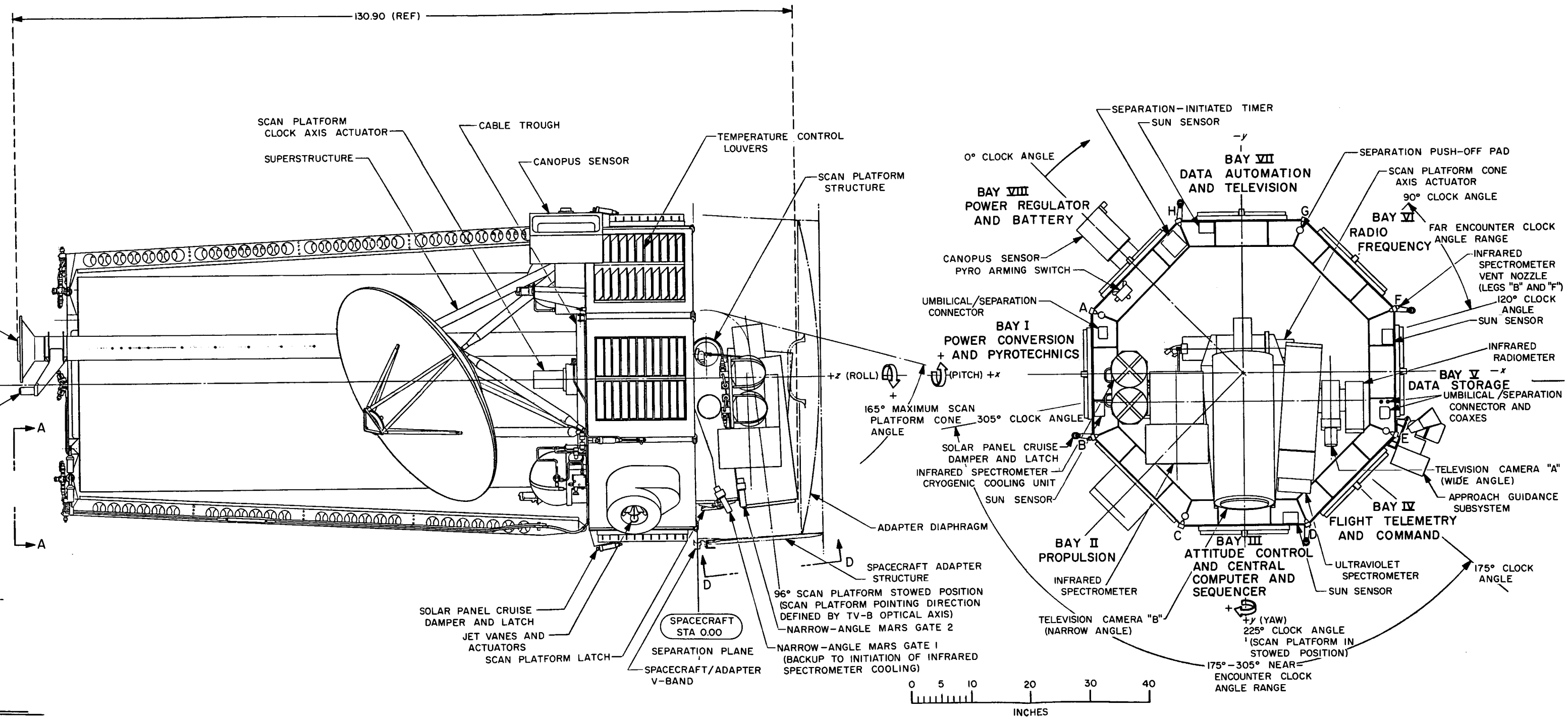

Fig. 1. *Mariner* Mars 1969 spacecraft mechanical configuration

LASSIFIED

UNCLASSIFIED

Antennas. The radio frequency subsystem low and high gain antennas are mounted on the spacecraft in a manner similar to the *Mariner* Mars 1964 design. However, the antenna configurations are different. The low gain antenna is longer, to be above the solar panels in the boost configuration, and has a conical end to shape its pattern to the 1969 trajectory. The high gain antenna is a circular parabolic dish, 40 in. in diameter. It is mounted in a fixed pointing position on a superstructure above the octagon.

Celestial sensors. The attitude control primary celestial sensors are located on the top of the octagon. The primary Sun sensors, for pitch and yaw control, are mounted on pedestals in Bays IV and VIII to provide coverage of the forward hemisphere. The Canopus sensor, for roll control, is located above Bay VIII on the centerline of the bay. A large baffle is attached to the end of the Canopus sensor to minimize its sensitivity to stray light. The Sun gate is mounted above Bay IV, viewing parallel to the spacecraft z axis. The secondary Sun sensors, for coverage on the aft hemisphere, are configured in four assemblies located in Bays I, III, V, and VII on the bottom of the octagon.

Attitude control gas assemblies. The gas assemblies, consisting of two mechanically interchangeable units, are mounted on the top of the octagon to provide a simple plumbing design and increased ease of installation and charging. Each gas assembly services gas jet manifolds on the tips of two adjacent solar panels.

Approach guidance. The approach guidance planet sensor is mounted on the outboard corner of the octagon between Bays IV and V. The instrument is located so that it can view Mars for 10 days before encounter.

Scan platform. The two-degree of freedom scan platform is mounted on the base of the spacecraft. The platform-pointed instruments are the infrared spectrometer and its cooling unit, ultraviolet spectrometer, wide- and narrow-angle television cameras, infrared radiometer, far encounter sensor, and two narrow-angle Mars gates. All the instruments are outboard of both platform gimbals, but are pointed in various directions to satisfy their particular objectives.

Spacecraft adapter and attachment/separation mechanism. The spacecraft attaches to the *Centaur* through a 21-in. high conical adapter which contains a diaphragm at its base for separating the spacecraft environment from that of the *Centaur*. Additionally, the adapter provides pads and mounting locations for separation connectors and separation-activated devices, separation mechanisms, and cabling. The spacecraft attaches to the adapter through a V-band release mechanism which is a reapplication of the *Mariner* Mars 1964 device.

3. Temperature Control of the Spacecraft System

a. General description.

Bus. The major features for the *Mariner* Mars 1969 thermal design for the bus are the same as for *Mariner* Mars 1964 and *Mariner* Venus 67. The bus is shielded, insofar as possible, from variable solar heating. Heat generated by the electronics is rejected mainly through variable emittance louvers located on all bays, except Bay II. The temperature differences between bays are minimized by providing good internal radiation and conduction heat paths.

Platform. The thermal design of the platform which orients the scientific instruments toward Mars is a significant departure from that flown on *Mariner* Mars 1964. The large size of the instruments and the two degrees of freedom for the platform movement have made it difficult to follow the *Mariner* Mars 1964 approach, i.e., to provide a good heat exchange between the bus and the platform. The approach selected, in effect, creates a second bus which is thermally independent from the main equipment compartment. The science platform (or science bus) will have a surface area of roughly 20 ft^2 which will be insulated as well as possible. This will minimize the amount of heat required to make up for unavoidable losses. Part of this power will be thermostatically controlled to compensate for the variations due to both uncertainties in the shielding and the switching on and off of the instruments.

Appendages. Structure and independently-mounted components external to the bus(es) are controlled passively, primarily by optical property control. Whenever possible, temperature-sensitive components are conductively coupled with the bus to maintain an acceptable temperature range (e.g., attitude control sensors). An exception is the approach guidance equipment which is mounted to the side of the bus between Bays IV and V. During the time this unit is not on, an equivalent amount of power will be supplied to a heater.

b. New design features.

Power profile. Significant changes in the amount, distribution, and sequencing of the spacecraft power have been made when compared to *Mariner* Mars 1964. While the *Mariner* Mars 1969 power totals are improved, the

UNCLASSIFIED

UNCLASSIFIED
CONFIDENTIAL

changes in power, particularly in Bays V and VII, will require more heat to be transferred within the bus. The power distribution within the bus is summarized in Table 1. The attitude control and science bays were exchanged from the *Mariner* Mars 1964 equipment arrangement to provide a more desirable power distribution during the cruise periods.

Scan platform. During the encounter modes, electrical power is switched to the instruments and actuators on the scan platform. To prevent the instruments from becoming too cold during the cruise phases, heat is supplied to the platform. Some of this heat is thermostatically controlled electrical DC power and the balance is provided by a radioisotope, Pm^{147}.

Launch environment. The launch vehicle for *Mariner* Mars 1969 will be an *Atlas–Centaur* used in a direct ascent trajectory. The ground cooling system used will be the same as used for the *Surveyor* launches. The ambient temperature within the shroud, prior to launch, will be maintained at 65–75°F (i.e., no prechill as attempted on *Mariner* Mars 1964).

The thermal environment will, for the most part, be similar to that experienced in *Mariner* Mars 1964 except for two conditions which result from the change to the *Centaur* launch vehicle and the direct ascent mode. The rate of pressure decay during the ascent period will be roughly four times (60 torr/sec) that previously experienced. Care must be exercised in the detail design of the thermal blankets to assure adequate venting during this period.

The second point of departure from the *Mariner* Mars 1964 environment is the aerodynamic heating of the spacecraft after the separation of the nose fairing. An initial heating pulse is determined by the timing of the nose fairing jettison and, for some launch times, a second heating period is experienced as a characteristic of the direct ascent trajectory. A maximum heating parameter has been established for each of these conditions, and corresponding constraints on the ascent sequence and trajectories

Table 1. *Mariner* Mars 1969 power distribution (February 1967), main equipment compartment

Bay No.	Bay equipment	Power dissipation, w				
		Earth cruise	Mars cruise	Mars encounter	Mars playback	Midcourse transient
I	Pyrotechnics	1.0	1.0	1.0	1.0	1.0
	Inverters	21.0	21.0	32.0	28.0	26.0
	Scan electronics	3.5	3.5	3.5	3.5	3.5
	Temperature control flux monitor	6.4	6.4	0	6.4	6.4
II	Midcourse propulsion system					High
III	Gyros + gyro electronics	2.0	2.0	2.0	2.0	11.6
	Attitude control electronics	5.0	5.0	5.0	5.0	16.0
	CC&S	17.5	17.5	17.5	17.5	17.5
IV	Command electronics	2.1	2.1	2.1	2.1	2.1
	Telemetry electronics	7.3	7.3	7.3	7.3	7.3
V	Tape transport	0	0	4.5	9.0	0
	Tape electronics	4.0	4.0	4.0	4.0	4.0
VI	RF communications electronics	21.5	21.5	21.5	21.5	21.5
	Power supply	7.5	7.5	7.5	17.0	7.5
	TWT amplifier	32.3	32.3	32.3	48.0	32.3
VII	TV electronics	0	0	24.0	0	0
	Data automation system	0	0	33.0	0	0
VIII	Booster regulator	20.0	20.0	30.0	26.0	24.0
	Power control	2.0	2.0	2.0	2.0	2.0
	Power source and logic	10.0	10.0	10.0	10.0	10.0
	Charge control (battery charger)	13.0	0	0	0	0
Totals		186.1	166.1	239.2	210.3	192.7

UNCLASSIFIED
CONFIDENTIAL

UNCLASSIFIED

have been imposed. The initial heating pulse will not exceed 140 lb/ft sec (0.18 Btu/ft² sec) and the subsequent peak will not exceed 30 lb/ft sec. (0.039 Btu/ft² sec). Under these conditions the upper shield will approach temperatures of approximately 300°F under the worst conditions.

4. Temperature Control Subsystem

General. For *Mariner* Mars 1969 the temperature control (TC) subsystem is defined by the hardware whose principal function is required to implement the spacecraft thermal design. At present this includes the thermally-actuated louver assemblies, the thermal shields, radioisotope heat sources, selected surface coatings, thermostat control elements, and an engineering experiment to measure the solar intensity.

Louver assembly. The *Mariner* Mars 1969 louver assemblies will be very similar to those used on *Mariner* Mars 1964. Nominally, the louver assembly will have an effective closed emittance of 0.12 and 0.76 when open. Considerable design flexibility exists with respect to the number of louver blades used and the opening temperature. A new provision for limiting the opening angle of the louvers allows them to be used more effectively on bays located below the solar panels, resulting in an increase in control capability for the louvers. An additional minor change of the support to the bearings permits the louver assembly to be installed on the spacecraft with all of the louver blades installed.

Thermal shields. As in *Mariner* Mars 1964, there will be two types of thermal shields used to reduce the heat losses from the spacecraft assemblies. Thin polished aluminum shields will be used where the surface area is small, the access to the assembly is frequent, and adequate structural support is available. Flexible multilayered shields will be used where the surface area is large, where the heat losses must be reduced to a minimum, and where it is impractical to provide structural support and damping for metallic shields.

Radioisotope heat sources. This heat source consists of a shielded sintered pellet of promethium oxide. It is 1.0 in. diameter, 1.1 in. long, and weighs 0.5 lb. The unit is loaded with enough Pm^{147} to produce 2.5 thermal watts and has a half-life of 2.6 yr.

Studies dating back to 1962 have evaluated various radioisotopes to be used as heat sources. Criteria of safety, availability, cost, and thermal watts per unit weight were used to compare various materials. Promethium was selected and a unit supplied by the AEC was evaluated at JPL in 1963. Concurrently, Atomics International developed a Pm^{147} heat source and is now supplying units for military use. A source similar to the military unit was also developed and qualified for the *Apollo* program; this source is planned for use on *Mariner* Mars 1969. It is shielded such that a radiation level of less than 0.5 mrad/hr at 1.0 ft will exist per unit. This level is considered very safe and does not impose additional operational constraints.

5. Mechanical Devices

The solar panel boost dampers for *Mariner* Mars 1969 are entering detailed design and have remained essentially unchanged in concept from the *Mariner* Venus 67 design. Past experience with this particular damping concept on *Mariner* Mars 1964 and *Mariner* Venus 67, and preliminary results of current investigations have helped to obviate some inherent problems peculiar to this design.

The dampers are designed to provide the following functions: tip-to-tip latching of the solar panels in the stowed position; damping of the natural vibration modes of the solar panels; and support of the static loads associated with the solar panels.

The larger and somewhat heavier solar panels of *Mariner* Mars 1969 have necessitated increases in the static spring rate to 40 lb/in. (versus 20 lb for *Mariner* Venus 67) and, in the maximum allowable stroke, to ±0.6 in. (versus +0.3 in. for *Mariner* Venus 67). The damper consists of two concentric tubes and a coaxial extension/compression spring, with a viscous damping fluid contained in the annulus by seals seated in the piston body. A central reservoir in the piston can supply fluid to the annulus to replace that which may have been removed by the wiping action of the seals. The damper configuration is shown in Fig. 2.

Past experience has shown that the cross-sectional squeeze on the seals is a critical parameter. Too little squeeze results in excessive leakage, too much in serious seal damage. Excellent results with minimum seal deformation have been obtained with a cross-sectional squeeze of approximately 20%. Several types of seals with cruciform cross sections (as opposed to the circular cross section of the conventional O-ring) are being investigated in an effort to eliminate the problem of seal spiraling and extrusion.

UNCLASSIFIED
CONFIDENTIAL

UNCLASSIFIED
CONFIDENTIAL

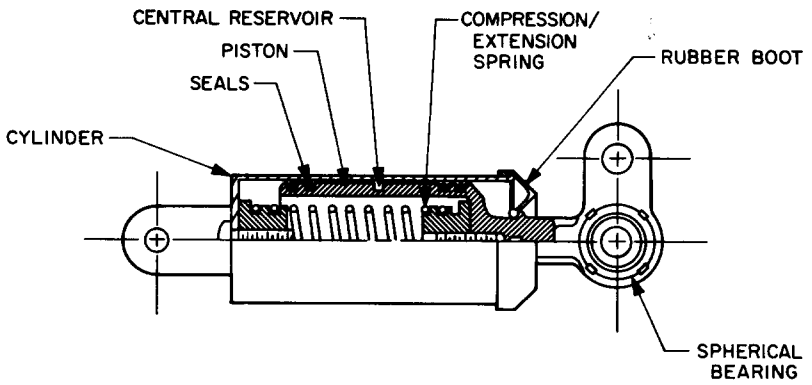

Fig. 2. Damper configuration

Theoretically, the damping force is provided by the shear stress generated in the annulus as the damping fluid flows relative to the cylinder. If such were the case, the damping force (assuming constant fluid viscosity) would be proportional to the velocity of excitation. Fig. 3 shows typical results obtained from testing a *Mariner* Venus 67 damper. The RMS damping force is plotted as a function of frequency at a fixed amplitude. A math model has been formulated in which the damping force is assumed to have a dual source: (1) shear stress generated in the annulus; and (2) the shear stress supported by the lubrication layer between the seals and the cylinder wall. Over the frequency range of 10 to 70 Hz and at an amplitude of ±0.025 in., the data points derived from the model lie within 10% of the observed test results. The model is presently being modified to include the spring characteristics of the seals and the deformation of the seals in the piston grooves in an attempt to account for the observed, constant phase angle between the damping force and the velocity of excitation.

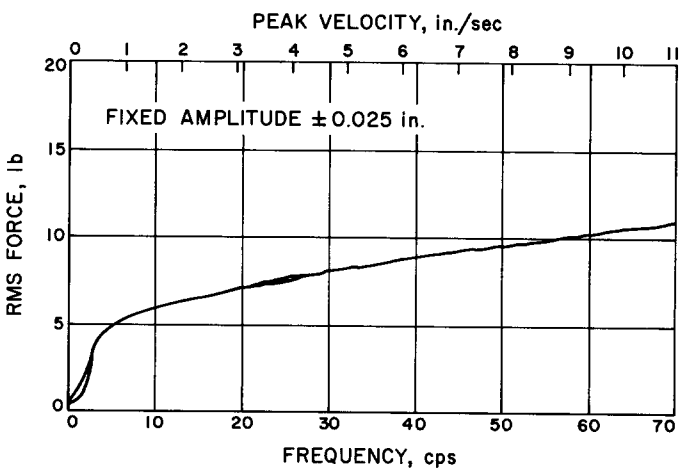

Fig. 3. Results from testing *Mariner* Venus 67 damper

6. Evaluation of Conversion Coatings for Magnesium Alloys

a. Introduction. Magnesium alloys, in general, exhibit poor resistance to corrosion, consequently protective coatings must be applied to avoid this problem. Two general types of coatings have been developed for use on magnesium, conversion and anodic, with one of the former (Dow-7) having been used on past *Mariner* spacecraft.

The primary purpose of the coatings used on magnesium is to offer protection against corrosion; however, the basic spacecraft design philosophy can dictate other requirements. In the case of past *Mariner* spacecraft, the coating was required to exhibit an emittance of 0.70 minimum for proper thermal control and was also to be conductive, thus providing a path for grounding of electronics through the spacecraft structure. Past experience with the Dow-7 proved its emittance to be difficult to control and its corrosion protection to be inadequate, requiring frequent "touch up" of corroded areas. Consequently, a program was initiated to evaluate other coatings for use on *Mariner* Mars 1969.

b. Program. An obvious solution to the above problem would be to use a coating of the anodic type since it exhibits corrosion resistance far superior to that of the conversion type[1]. In addition, emittance is controllable by increasing thickness, as shown in Fig. 4. However, the anodic coatings are dielectric in nature, thus do not meet the conductivity requirement for the grounding of electronic equipment. Therefore, conversion coatings which are more conductive were investigated in an attempt to provide one superior to Dow-7.

[1]Personal communication with Dr. J. Stevens, Dow Chemical Company, Metal Products Department, Midland, Michigan, and with B. Cohen, Air Force Materials Lab, Wright-Patterson AFB, Ohio.

UNCLASSIFIED
CONFIDENTIAL

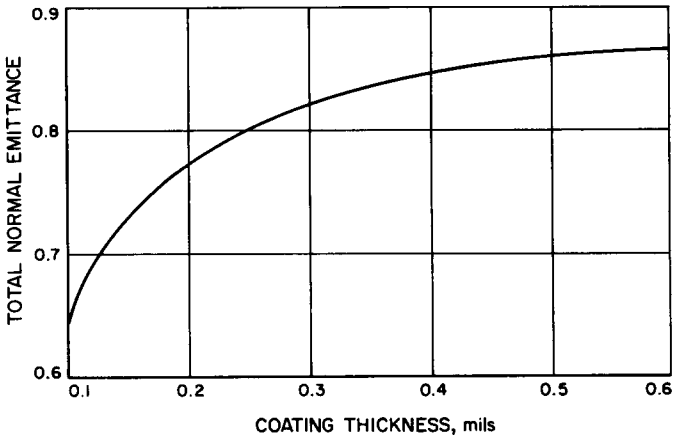

Fig. 4. Coating thickness versus total normal emittance for Dow-17

Three conversion coatings (Dow-9, Dow-23, and Iridite-15) were selected on the basis of available information (Refs. 1–3). Dow-7 was included in the program to provide a control for comparison. The coatings were applied to the two alloys used on the spacecraft, ZK60 and AZ31, each being represented with a grit blasted and an as-machined surface. Each coating was applied by different immersion times, using the optimum time t for each, as well as $t/2$ and $2t$.

Specimens representing each variable mentioned were prepared for corrosion, emittance, and resistance measurements. Thickness of representative samples was determined using a permascope and was verified by microscopic measurements. The data appear in Table 2. It is apparent from the table that conversion coatings do not linearly increase in thickness as immersion time is increased. Also, the outer portion of the coatings tends to become powdery with increasing thickness.

Contact resistance was determined, per MIL-C-5541. Due to the soft nature of conversion coatings, representative resistance measurements were difficult to obtain. The values varied erratically, as shown in Table 3, however, all were considerably lower than anodic coatings. Iridite-15 consistently exhibited the lowest values.

Corrosion tests were conducted at a temperature of 100°F and a relative humidity of 95%. All specimens were left in the humidity chamber for 7 days, periodically being inspected for signs of corrosion. The corrosion protection afforded by the conversion coatings is minimal, corrosion being observed on some samples after only 2 days in the chamber. In addition, such coatings are not durable for handling purposes. Dow-9, Dow-7, and Iridite-15 exhibited the best protection of those tested, with Dow-23 being considerably poorer.

Table 2. Thickness data for as-machined samples

Coating	Base	Immersion time, min	Thickness, in.[a] (permascope)	Thickness, in. (microscopic)
Dow-7	ZK-60	7	0.00015	—
		15	0.00022	0.00020
		30	0.00022	—
	AZ-31	15	0.00010	—
		30	0.00020	—
		60	0.00022	—
Dow-9	ZK-60	10	0.00030	—
		20	0.00020	0.00021
		40	0.00027	—
	AZ-31	10	0.00015	—
		20	0.00017	—
		40	0.00027	—
Dow-23	ZK-60	15	0.00013	—
		30	0.00022	0.00006[b]
		60	0.00032	—
	AZ-31	15	0.00022	—
		30	0.00037	—
		60	0.00027	—
Iridite-15	ZK-60	0.5	0.00020	—
		1	0.00020	0.00018
		2	0.00022	—
	AZ-31	0.5	0.00025	—
		1	0.00026	—
		2	0.00025	—

[a]Average of individual readings from two separate permascopes.
[b]This value was the measured coating thickness. However, a gap existed between the coating surface and the mounting material, indicating possible loss of some coating material during polishing. The distance from the base alloy to the mounting material was approximately 0.00020 in., which agrees with the permascope.

Emittance measurements were made at two sources. Table 4 compares the emittance of the coatings under like conditions and for the optimum immersion time of each. Dow-7 and Dow-23 exhibited the highest values; however, it should be noted that Dow-9 on ZK60 is also high, as can be seen in Table 5, where the effects of immersion time and base material are shown. It is evident in the tables that emittance can be altered by increasing thickness, however, close control of the process is difficult. Dow-23 showed the highest emittance obtained; whereas, Dow-9 gave a wide variation in emittance between substrate materials. The appearance of the coatings varied with

UNCLASSIFIED
CONFIDENTIAL

Table 3. Resistance data for coatings evaluated

Coating	Base	Pretreatment of surface	Immersion time, min	Side A resistance[a]	Side B resistance[a]	Coating	Base	Pretreatment of surface	Immersion time, min	Side A resistance[a]	Side B resistance[a]
Dow-7	ZK-60	As-machined	7	0.0030	0.0225	Dow-23	ZK-60	As-machined	15	0.180	0.377
			15	0.147	0.0050				30	0.046	0.066
			30	0.517	0.173				60	0.0095	0.0127
		Grit blasted	7	0.0190	0.0415			Grit blasted	—	—	—
			15	0.0310	0.0106				30	0.0135	0.0105
			30	0.637	0.563				60	0.0052	0.0082
	AZ-31	As-machined	15	0.250	0.565		AZ-31	As-machined	15	0.0058	2.00
			30	9.5	1.4				30	0.0520	0.0433
			60	39.0	9.5				60	0.0007	0.0029
		Grit blasted	15	0.0450	0.0320			Grit blasted	15	0.0011	0.0009
			30	0.327	2.03				30	0.0009	0.0019
			60	3.85	10.5				60	0.0071	0.0100
Dow-9	ZK-60	As-machined	10	0.380	0.245	Iridite-15	ZK-60	As-machined	0.5	0.0425	0.0310
			20	0.113	0.057				1	0.0065	0.0048
			40	0.157	0.069				2	0.0500	0.0036
		Grit blasted	10	0.0084	0.0031			Grit blasted	0.5	0.0155	0.0026
			20	0.0760	0.335				1	0.0133	0.0180
			40	0.510	1.10				2	0.0018	0.0096
	AZ-31	As-machined	10	0.083	0.320		AZ-31	As-machined	0.5	0.082	0.383
			20	0.064	0.043				1	0.0443	0.1005
			40	0.036	0.210				2	0.155	0.063
		Grit blasted	10	0.117	0.065			Grit blasted	0.5	0.0170	0.0865
			20	0.045	0.130				1	0.0850	0.0610
			40	0.061	0.133				2	0.0400	0.0380

[a]Resistance in ohms.

Table 4. Comparison of total normal emittance for conversion coatings processed at their optimum immersion times

Coating	Base	Pretreatment of surface	Immersion time, min	ε_N (Source A)[a]	ε_N (Source B)[b]
Dow-7	AZ-31	As-machined	30	0.64	0.70
Dow-9			20	0.33	0.39
Dow-23			30	0.78	0.82
Iridite-15			1	0.62	0.61

[a]Source A used the Perkin-Elmer spectrophotometer.
[b]Source B used the Gier-Dunkle reflectometer.

base alloy composition, with Dow-9 and Iridite-15 showing the widest variations and being very light in color on ZK60 and dark on AZ31.

c. Conclusions. From the test information obtained, it can be concluded that none of the conversion coatings evaluated exhibits a combination of properties better than that exhibited by Dow-7. Therefore, no appreciable gain can be obtained by using another conversion coating in lieu of Dow-7.

d. Recommendations. Because of the difficulties experienced in using Dow-7 in past programs, it is felt that anodic coatings should be considered for future use on magnesium parts. Corrosion protection is better and emittance can be controlled when using such coatings. Only electrical continuity must be provided due to the nonconductive nature of anodic coatings, however, this could be accomplished by providing an electrically conductive path, i.e., through the mechanical fasteners which attach the parts together.

UNCLASSIFIED
CONFIDENTIAL

UNCLASSIFIED

Table 5. Emittance data for conversion coatings using various processing techniques

Coating	Base	Pretreatment of surface	Immersion time, min	ε_N (Source A)[a]	ε_N (Source B)[b]
Dow-9	AZ-31	As-machined	20	0.33	0.39
	ZK-60	Grit blasted	20	0.53	—
			40	0.86	—
Dow-23	AZ-31	As-machined	15	0.61	—
			30	0.78	0.82
			60	0.79	—
		Grit blasted	15	0.78	—
			30	0.80	—
			60	0.79	—
	ZK-60	As-machined	15	0.68	—
			30	0.74	—
			60	0.76	—
		Grit blasted	15	—	—
			30	0.82	—
			60	0.88	—
Iridite-15	AZ-31	As-machined	1	0.62	0.61
	ZK-60	As-machined	1	0.42	0.39
		Grit blasted	1	0.29	0.36

[a]Source A used the Perkin-Elmer spectrophotometer.
[b]Source B used the Gier-Dunkle reflectometer.

C. Guidance and Control

1. Spacecraft Control

The definition of interface circuits for the attitude control, approach guidance, and scan control is complete,and the end circuits on spacecraft circuit data sheets have been signed off.

The preliminary parts lists for the attitude control, approach guidance, and scan have been submitted to Project Reliability Assurance.

All design drawings have been released for the thrust vector control assembly which includes jet vane actuators with jet vanes, the actuator mounting ring, and the thermal shield. Documentation of the attitude control subsystem has progressed to the level where 20% of the design drawings and 26% of the detail specifications are released.

Design room activity has started on the scan control assemblies and subassemblies, including three scan electronics subassemblies, narrow-angle Mars gate, far-encounter planet sensor and scan actuator.

Presentations have been made for the attitude control subsystem preliminary design review. These presentations concentrated on Canopus sensor design, repackaging of the gyro control subassembly and the attitude control electronics subassembly, configuration changes on the gas system, and thrust vector control assembly design.

The major design effort for the attitude control has been the redesign of the Canopus sensor. This redesign includes a roll plate loop mechanization, an adaptive low gate which periodically adjusts the brightness criteria for acquisition, a new Canopus sensor power logic which turns on Canopus sensor power with attitude control turn on, and a new baffle and optical design to protect against stray light in the new location of the Canopus sensor.

Information for the approach guidance interface control drawing has been received from Electro-Optical Systems and has been submitted to project for the generation of the drawing. Interface control drawings for the attitude control and scan are being generated with the design package.

2. Gyro Control Subassembly

The redesign effort on the gyro control subassembly is progressing at a reasonable rate. This effort includes the following items:

(1) Increase of over-all height 0.4 in. to accommodate the new spacecraft Case III redesign.

(2) Reorientation of the pitch and yaw gyro input axes to accommodate the move from Bay VII to Bay III.

(3) Remount all connectors in such a way as to allow assembly of the harness externally, and to allow blind insertion into the new spacecraft body-fixed connector mates.

(4) Relocation of the elapsed time indicator.

(5) Increased alignment accuracy of the gyros by referencing dimensions differently.

(6) Repackage of command current regulators and voltage regulators to reduce AC pickup and eliminate spikes on the outputs.

CONFIDENTIAL UNCLASSIFIED

UNCLASSIFIED
CONFIDENTIAL

(7) Re-layout of all electronic modules to reduce crowding and eliminate existing interferences.

All drawings for the gyro control subassembly from the *Mariner* Mars 1964 program are being redrawn. This was necessary to standardize all drafting on the program so that the subsystem contractor would be able to perform the fabrication effort with a maximum amount of reliability and efficiency, and with a minimum amount of rework. Twenty-seven specifications are being written to cover the building and testing of the flight hardware and the test equipment. This effort represents a major increase from *Mariner* Mars 1964.

The drafting effort is approximately 80% completed. Preliminary copies of all drawings have been supplied to the contractor and a set of released drawings for the capacitor subassembly is now ready for transmittal. Released drawings for the gyro and electronics subassemblies and the top assembly drawings are expected to be completed in March. Vellums of these drawings are being transmitted to the contractor, and drafting changes and change control procedures will be conducted by him from that point on. The specification effort is about 70% complete at this time. Ten specifications have been released to date and vellums have been transmitted to the contractor. It is expected that this effort will be completed in April.

The effort on the test equipment is approximately 60% complete at this time. One GCA bench test set has been delivered to the contractor to date, along with copies of all drawings for this equipment. Other drawings necessary for the fabrication of test equipment are to be generated by the contractor as he requires them. The calibration and maintenance specification for this rack is now released and the test specification for use of this equipment is expected to be released in March. Two of the four sets of test equipment, along with all necessary drawings, have been delivered to the gyro manufacturer; the remaining two sets will be ready for delivery in March.

All electronic components have been defined at this time and copies of procurement and screening specifications have been transmitted to the subsystem contractor, along with authorization to buy. Procurement activity is now under way by the contractor. Final definition of all mechanical components and materials is now being completed and specifications written.

The gyro procurement is progressing according to schedule with the first units expected during the first week of June. Drawings and operation sheets have been completed by the gyro vendor, and orders have been placed for all components. Fabrication is complete on approximately 23 motors and 8 motor and float assemblies at this time. Other fabrication efforts are progressing similarly. The final reliability and QA plans have been received and approved by JPL and a JPL QA engineer has been in residence at the vendor's facility since the first week of January. He will remain in residence until the completion of the contract.

3. Scan-Control Subsystem

The scan platform provides a mounting base for some of the scientific equipment used during encounter of the *Mariner* Mars 1969 spacecraft and the planet Mars. The platform is mechanized with two degrees of freedom, in clock, which is defined to be coincident with the spacecraft roll axis, and in cone, which is orthogonal to the roll axis. The scan platform performance is divided into two modes: far encounter, and near encounter. The scan control subsystem is comprised of two gimbal servo drivers (cone and clock), four stepper motor-driven potentiometers (allowing for the prestorage of four discrete reference-angle positions), a far-encounter planet sensor (FEPS), and mode-control electronics.

Fig. 5 is a block diagram representation of the scan control subsystem. A detailed discussion of this block diagram follows.

The angular reference assembly is powered during the cruise phase of the mission. The rest of the subsystem remains deenergized until the encounter sequence begins. The far-encounter cone and clock reference angle positions have no provisions for inflight updating. The near-encounter cone and clock angle positions are updateable through the use of ground-originated quantitative commands, labelled QC in Fig. 5. Telemetry points are provided for the clock and cone near encounter reference potentiometers, to verify the system response to the updating commands.

The four position-storage devices (potentiometers) are updated on the launching pad to place the platform positions in both far- and near-encounter modes to correspond to the predicted nominal spacecraft trajectory. Referring to Fig. 5, the four potentiometers are identified

UNCLASSIFIED
CONFIDENTIAL

CONFIDENTIAL

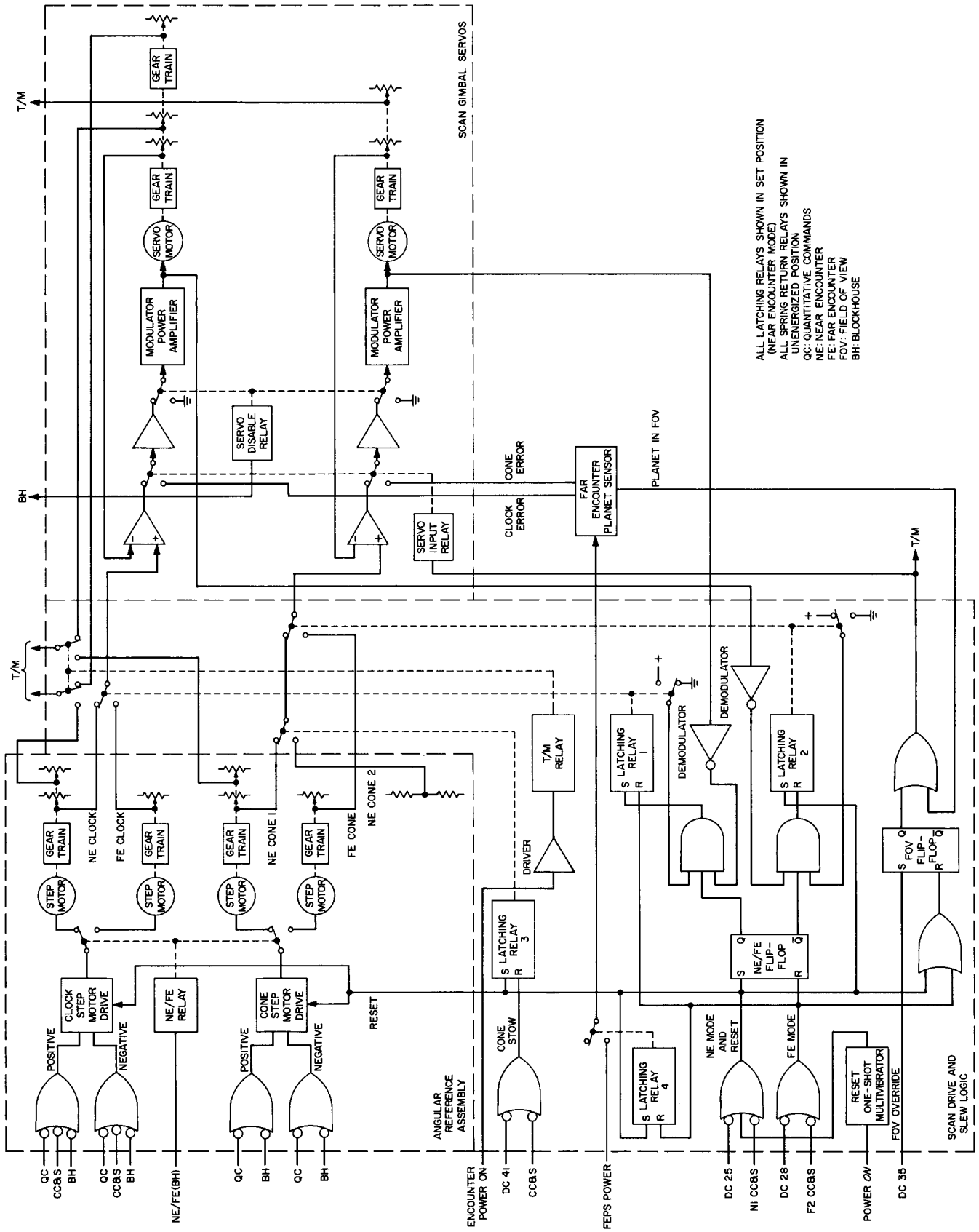

Fig. 5. Block diagram of scan platform subsystem

CONFIDENTIAL
UNCLASSIFIED

UNCLASSIFIED
CONFIDENTIAL

within the dotted block termed angular reference assembly. Two stepper motor-drive units are identified, one for clock and one for cone. Using blockhouse-access cabling, a relay is energized to select the desired pair of potentiometers (far or near encounter), and the reference positions of these potentiometers are updated by introducing the appropriate number of pulses into either the clockwise or the counterclockwise leads to the motor drive. These terminals are labelled BH (blockhouse) in Fig. 5. The angular reference assembly is mechanized to receive pulses at the rate of 1 pps, each pulse to correspond to an equivalent 1-deg increment in the platform position.

a. Far encounter. Encounter is defined as that point in time at which the spacecraft reaches the point of closest approach to Mars. Far encounter is defined to occur over a period of time starting at encounter −48 hr, and ending at encounter −12 hr. Fig. 6 is a gross, not-to-scale, two-dimensional representation of the Sun–spacecraft–planet configuration. Two positions of the spacecraft are identified to correspond to its location at the beginning and the end of the far-encounter phase.

The far-encounter mode is initiated by a central computer and sequencer (CC&S) signal causing the unenergized parts of the scan subsystem to be powered, and causing the platform to slew from its stowed position to the prestored, near-encounter position. An hour later, at encounter −47 hr, another CC&S signal causes the platform to slew to the prestored, far-encounter position. It should be noted here that, due to structural interference problems, the platform must traverse the angular distance from the nominal near encounter to the nominal far encounter in an ordered, sequenced manner. Specifically, clock slewing is to precede cone slewing when moving from the near- to the far-encounter position; the sequence is reversed when slewing from the far- to the near-encounter positions. The dotted block labeled "mode control electronics" controls the slew sequencing. A subsequent article will deal with the sequencing circuitry in detail.

The positioning of the platform in the prestored far-encounter angles, assuming that the trajectory is within the predicted dispersions, will cause the planet to appear within the FEPS field of view. The FEPS will have a ±5-deg field of view in both clock and cone angles. The appearance of the planet in the FEPS field of view will result in a logic-level signal, causing the control of clock and cone gimbal servos to be switched from the reference potentiometers to the FEPS. Feedback lines from the clock and cone gimbal position potentiometers are opened. The

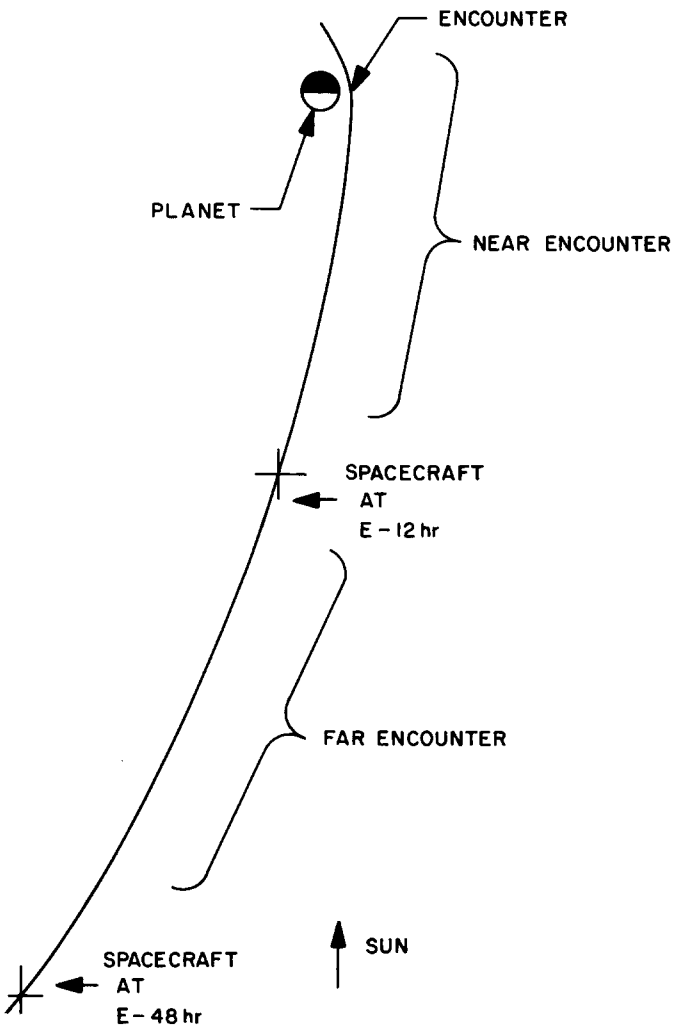

Fig. 6. Two-dimensional representation of Sun–spacecraft–planet configuration at encounter

loops are now closed through the location of the planet in the FEPS field of view. The FEPS generates error voltages proportional to the displacement of the planet from the center of its field of view in both cone and clock. The servo system is driven to maintain these error voltages around null, and thus maintain the planet centered in its field of view. Effectively, the motion of the platform shall compensate for the limit-cycle characteristics of the spacecraft and for the apparent movement of the planet due to the spacecraft's travel on its trajectory. The platform-mounted scientific instruments thus remain pointed at the center of the illuminated portion of the planet. This mode is maintained until encounter −12 hr.

b. Near encounter. At encounter −12 hr, a CC&S signal causes the FEPS to be disabled, reactivates the local feed-

UNCLASSIFIED
CONFIDENTIAL

UNCLASSIFIED

back paths from the clock and cone gimbal-position potentiometers, and drives the platform back to the prestored, near-encounter position.

Should the latest available trajectory information warrant it, the near-encounter clock and cone angles may be updated up until encounter −4 hr. The platform does not perform any dynamic tracking during the near-encounter phase. It is driven to several discrete positions as described in the following.

Subsequent to encounter − 4 hr, the platform remains fixed until the path traced out by the line of sight of the platform-mounted instruments crosses the planet limb. At some time after limb crossing, a time that is selected by the CC&S to occur between shuttering of the TV camera, a CC&S signal inputs a number of pulses into the angular reference assembly causing the near-encounter clock-reference potentiometer to be driven a fixed angular increment corresponding to the number of pulses introduced. The clock servo driver will drive the clock gimbal to follow the potentiometer voltage.

Some time later, expected to be measured in minutes, a CC&S signal will cause the input to the cone gimbal servo driver to be switched from the potentiometer to a fixed reference voltage, causing cone gimbal to be driven to a prestored, fixed position. Fig. 7 shows the path traced out by a hypothetical line fixed with respect to the platform.

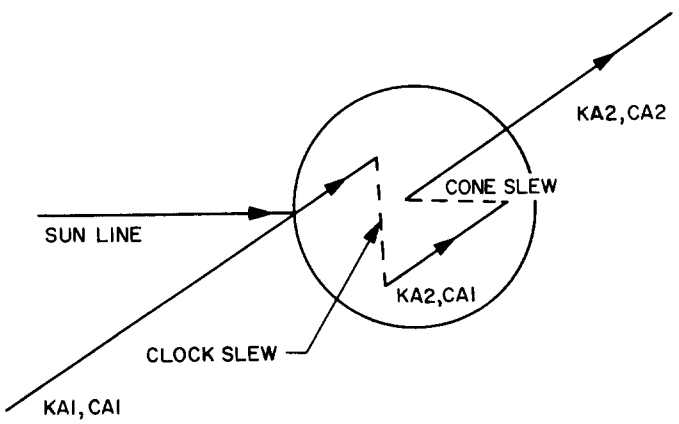

Fig. 7. Scan generated by Clock 1, Cone 1; Clock 2, Cone 1; and Clock 2, Cone 2 at near encounter

After the line of sight of platform-mounted instruments crosses the dark planet limb, power is shut off to the scan subsystem, thus terminating its functional performance.

D. Propulsion

The *Mariner* Mars 1969 spacecraft propulsion subsystem will provide the necessary impulse to remove or reduce injection dispersion errors so that a Mars flyby with a sufficiently small miss distance can be reasonably assured.

It is planned that the propulsion subsystem will be very similar to that used on the *Mariner* Mars 1964 spacecraft. The propulsion subsystem utilizes a liquid monopropellant, anhydrous hydrazine, as the propellant. It is functionally a constant-thrust rocket with the propellant pumped by pressure-regulated gas. Principal components consist of a high-pressure gas reservoir, a pneumatic pressure regulator, a propellant tank and bladder, valves, and a rocket engine. The rocket engine contains a catalyst to maintain the decomposition of hydrazine.

During the period since the last report (SPS 37-42, Vol. II), proposals for the fabrication of the *Mariner* Mars 1969 propulsion subsystem were received from industry and evaluated. On February 22, 1967, a contract was awarded to TRW Systems. This contract covered the first phase of the effort, generation of appropriate documentation. The documentation includes quality assurance and reliability plans, manufacturing flow plans, and detail and environmental test specifications.

Simultaneous with the contract evaluation and negotiation effort, JPL's Propulsion Division proposed to the *Mariner* Mars 1969 Project Office use of the Shell #405 spontaneous catalyst[2] in place of the bipropellant start system employed in *Mariner* Mars 1964. Upon approval of the change by the Project Office, the necessary design changes were initiated.

In the *Mariner* Mars 1964 propulsion subsystem decomposition of the hydrazine is initiated by injecting a small amount of nitrogen tetroxide (contained in the oxidizer start cartridge) into the thrust chamber during startup. The hypergolic reaction of the nitrogen tetroxide and hydrazine heats the catalyst contained in the thrust chamber to a temperature which will sustain the monopropellant reaction. The Shell #405 catalyst spontaneously initiates hydrazine decomposition at propellant

[2]Developed by the Shell Development Company.

UNCLASSIFIED CONFIDENTIAL

temperatures down to freezing, and at catalyst bed temperatures down to about zero degrees Fahrenheit. As a result, with the spontaneous catalyst, the oxidizer start cartridge, carried on *Mariner* Mars 1964, can be deleted, making a simpler system.

Fig. 8 is a cross-sectional view of the *Mariner* Mars 1964 hydrazine reactor (thrust chamber). The reactor is fabricated from Haynes high temperature alloy, and is of relatively straightforward construction, which includes conventional machining and heliarc welding. It incorporates dual propellant inlets – one for oxidizer and one for fuel. The entire catalyst bed consists of 3/16-in. spheres of the JPL Type H-7 catalyst. The injector assembly consists of four oil burner-type spray nozzles through which the fuel is injected, and one central oil burner spray nozzle through which 15 cm^3 of oxidizer are sprayed at the initiation of the firing process. The ensuing bipropellant reaction (the hydrazine fuel and the N_2O_4 oxidizer are hypergolic, i.e., they spontaneously ignite) lasts for several hundred milliseconds and releases enough energy to heat the nonspontaneous catalyst to a temperature such that the monopropellant decomposition is sustained.

The replacement reactor is shown in Fig. 9. Note that the catalyst bed is different. The top 0.2 in. consists of 20–30 mesh Shell #405 catalyst, and the lower portion consists of 1/8-in. cylinders of the same catalyst. Tests are being made to explore the possibility of packing a portion of the lower bed with the JPL Type H-7 catalyst to minimize the loss in performance. The injector of this engine consists of forty-two 0.017-in. diameter holes. The catalyst bed is slightly smaller in diameter than the previous reactor and considerably shorter (about 2.2 in.). The fuel enters through a single inlet and is sprayed through the small holes on to the top of the catalyst bed. The same materials and construction techniques have been used as those for *Mariner* Mars 1964. An identical nozzle assembly is also used in order that the jet vane interface will not be disturbed. In addition, the bolt circle at the top of the reactor remains the same as that used on *Mariner* Mars 1964. The reasons for these materials and interface considerations are probably self-evident; it was

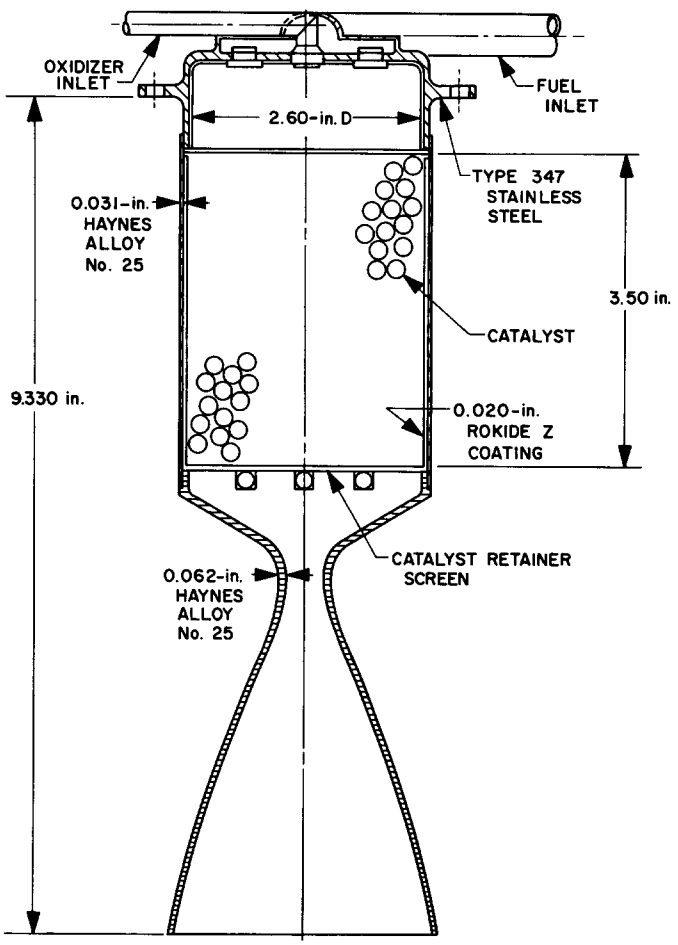

Fig. 8. Cross section of bipropellant start engine

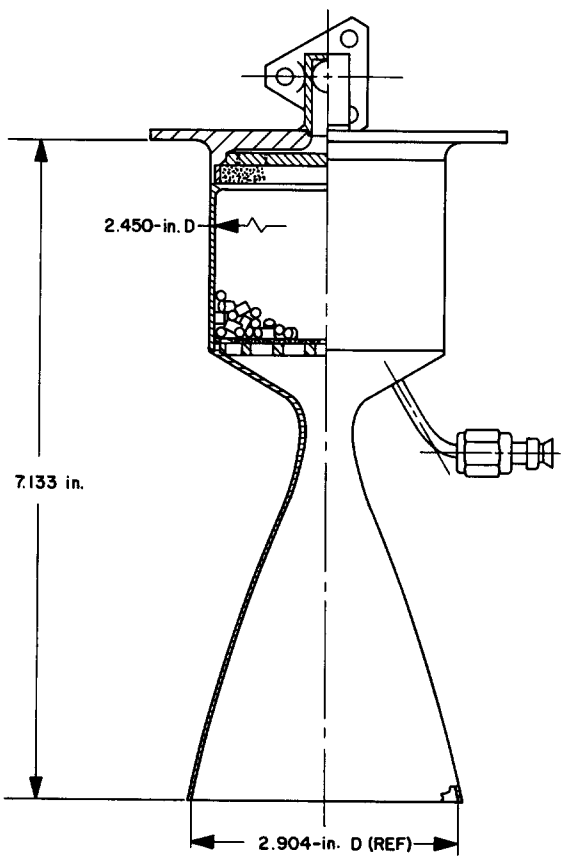

Fig. 9. Shell #405 catalyst, 50-lb thrust reactor

UNCLASSIFIED

desired not to introduce new materials or fabricating techniques in this engine, nor to disturb the existing jet vane and substructure interfaces.

Figs. 10–12 show how the new reactor operates as compared with the previous reactor. Fig. 10 is the start transient from a 50-lb thrust JPL H-7 catalyst engine (*Mariner* Mars 1964 design). As can be seen, there is a fairly rapid initial rise in chamber pressure (which is directly proportional to thrust for these purposes) to about 130 psia, a slight drop off, and then the pressure again starts to rise toward the steady-state value of 186 psia, having reached 171 psia at the end of about 40 msec. Fig. 11 shows the start transient from a 50-lb thrust spontaneous catalyst engine. Note here that there is a moderate overshoot to 176 psia upon initiation of decomposition, with a moderate drop off followed by a rather rapid rise to 174 psia at 40 msec. If we place one of these plots on top of the other, the differences in start characteristic are insignificant as viewed in a very short time scale. Fig. 12 is a comparison on a longer time scale (about 30 sec). In this case, one can observe that the spontaneous catalyst design has a faster rise time to a

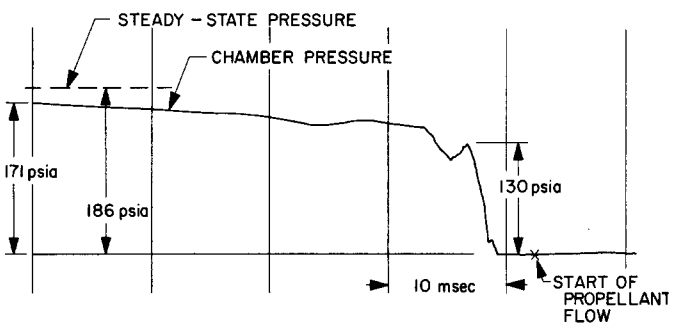

Fig. 10. Start transient from 50-lbf JPL H-7 catalyst, Test 560, *Mariner* Venus 67

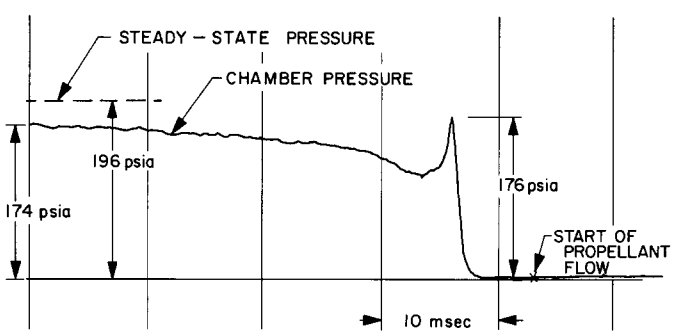

Fig. 11. Start transient from 50-lbf spontaneous catalyst, Test 566, *Mariner* Mars 1969

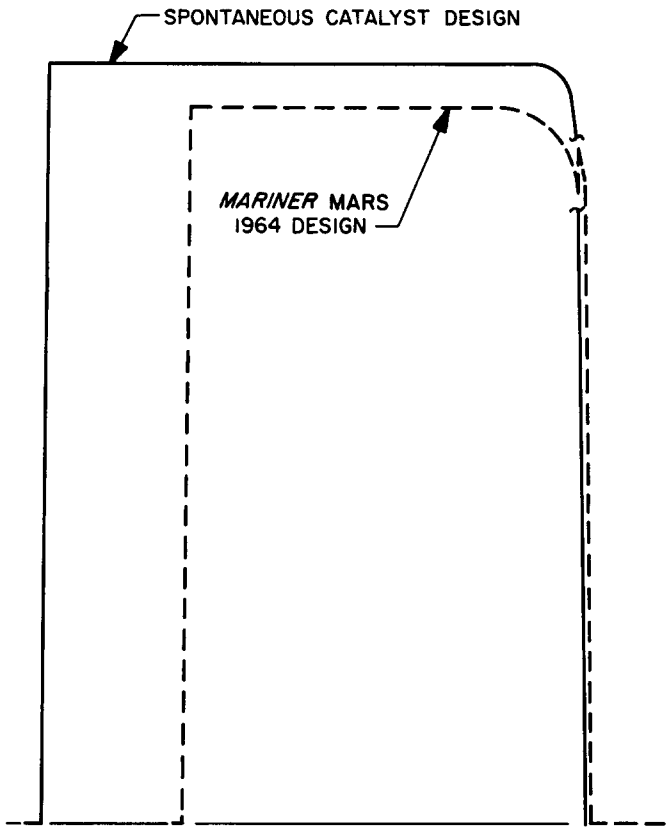

Fig. 12. Comparison of pressure–time curves

steady-state value than the *Mariner* Mars 1964 design. It is attributed primarily to the lower total heat capacity of a spontaneous catalyst engine. The pressure trace on the *Mariner* Mars 1964 design shows an immediate rise, then slight decrease immediately at ignition. On this time scale one is observing the bipropellant ignition during that first part of a second. The pressure then begins a slow climb to a steady-state value. It is concluded that there is little difference in the transient operation of these engines. If anything, the spontaneous catalyst engine permits better predictability of the thrust time curve, since it approaches steady-state operation more rapidly.

A schematic diagram of the *Mariner* Mars 1964 propulsion system is shown in Fig. 13. The principal components consist of the high-pressure nitrogen tank, explosive valve assemblies, nitrogen pressure regulator, propellant tank and bladder, rocket engine, and oxidizer start system. The oxidizer start system consists of two separate bellows cartridges, each containing about 15 cm^3 of nitrogen tetroxide oxidizer. Nitrogen gas under 400 psi pressure is used to compress these bellows and force the oxidizer into the engine. Shown on this schematic are two

UNCLASSIFIED

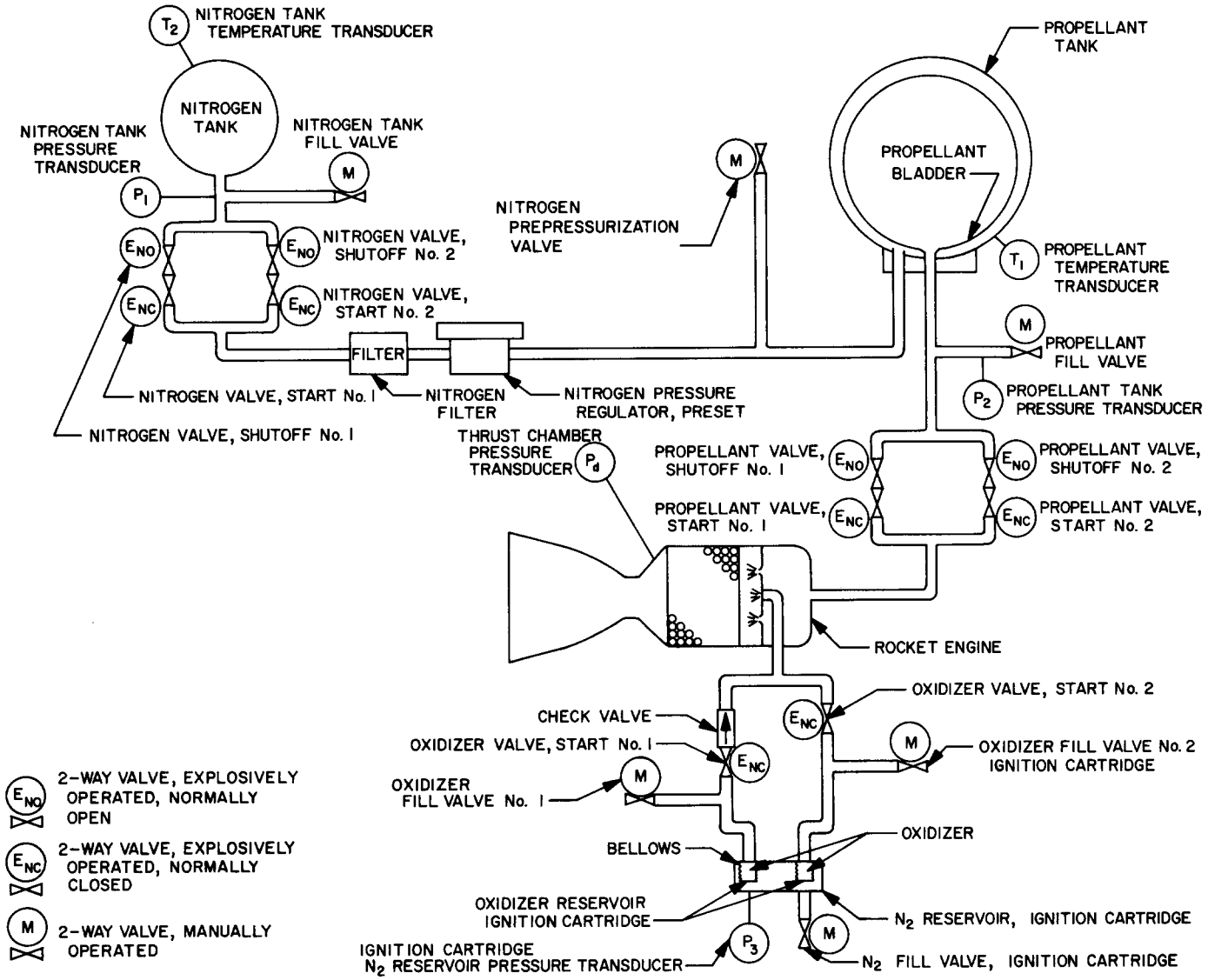

Fig. 13. Schematic of *Mariner* Mars 1964 propulsion subsystem

UNCLASSIFIED

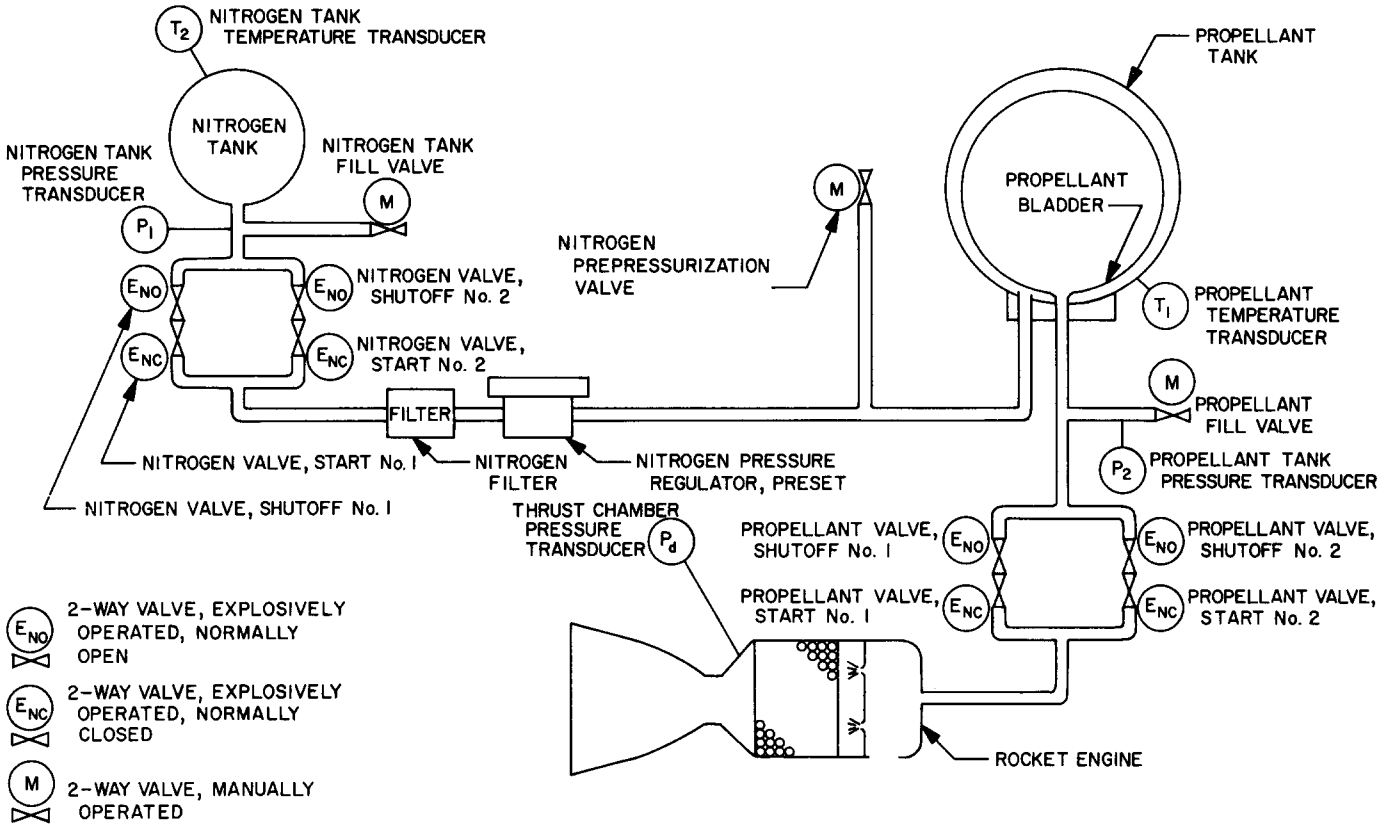

Fig. 14. Schematic of spontaneous catalyst propulsion subsystem

oxidizer fill valves, a nitrogen fill valve, a nitrogen reservoir pressure transducer, two normally-closed explosive valves, and a check valve to prevent back flow of oxidizer during the actuation of the right-hand circuit. In all, there are eight major components shown on the oxidizer start system. This compares with 19 other major components on the balance of the propulsion system, excluding plumbing and structure.

Fig. 14 is a schematic of the spontaneous catalyst subsystem. This schematic is identical to the previous one for *Mariner* Mars 1964, except for the deletion of the oxidizer start cartridge. It is significant to note that all the existing technology used in the nitrogen tank circuit, the propellant circuit, etc, remains intact.

Table 6 is a compilation of the spacecraft functional changes resulting from conversion to Shell catalyst. The significant changes are in the propulsion system and include a new engine assembly with a slightly lower performance, and improved impulse accuracy. Changes to the balance of the spacecraft are very small, and are itemized in the table.

Table 6. Functional changes resulting from conversion to Shell catalyst

1. Propulsion: New engine assembly; delivered performance lower by about 1%	
2. Pyro: Elimination of the requirement to fire two squibs; Simpler cabling and OSE; Eight additional connector pins available	
3. Data encoder: One additional channel available	
4. CC&S	No changes
5. Power	
6. Attitude control	

Table 7 shows a few of the significant failure modes, most of them pertaining to the reactor assembly itself. The significant thing to be noted from the comments on this table is that, under any of the conditions shown here (and these are the important ones), in no case will the spontaneous catalyst engine give a catastrophic failure. Experience with reactors of this type indicates that if,

UNCLASSIFIED

UNCLASSIFIED
CONFIDENTIAL

Table 7. Comparison of failure modes

Failure	Results	
	Existing system	Spontaneous catalyst
Leakage of oxidizer or oxidizer pressurant	Reactor fails to start; No ΔV; mission failure	No oxidizer required N/A
Catalyst is degraded	Rough operation; mission slightly degraded	Delayed start, rough operation, mission degraded
Catalyst becomes inactive	Highly unlikely; short pulse only would result	Unlikely; reactor would not operate; mission failure
Sequencing of fuel and oxidizer flow abnormal	Slight delay O.K. Longer delay results in reactor exploding	N/A
Oxidizer check valve fails	No ignition	N/A

for any reason, the catalyst or engine does not operate properly, then the result is simply rough operation, or no operation at all. As is known, this is not the case with the bipropellant start system. In the event of a couple of failure modes, an engine explosion would occur.

Table 8 is a summary of the relative merits of the existing system compared to a spontaneous catalyst system. It is believed that the new system will increase reliability greatly, but it has not been flight-proven. The presence of 19 components, compared to 27, and 10 leak paths, compared to 18 in the *Mariner* Mars 1964, implies a decrease in the system unreliability by about one-third, which is a significant improvement. In addition, there is an estimated weight savings of 4.6 lb.

Table 8. Summary of relative merits of existing system and spontaneous catalyst system

Consideration	*Mariner* Mars 1964 design	Spontaneous catalyst design
Reliability	1. A proven design, successfully employed on all *Ranger* and *Mariner* flights to date (7 different spacecraft)	Not flight-proven; several new programs are employing these reactors, but using smaller sizes. Except for oxidizer start cartridge and reactor, system is identical to that of *Mariner* Mars 1964.
	2. Requires at least 10 cm^3 of oxidizer to start reliably. Four liquid leak paths; 1 gas	No oxidizer required; no leak paths
	3. 27 components 18 leak paths	19 components 10 leak paths 30% fewer components 45% fewer leak paths
Weight	Present system weight: 51.1 lbm	Spontaneous catalyst system weight: 46.4 lbm Savings: ~4.6 lbm

References

1. White, E. L., and Fink, F. W., "Corrosion Protection of Magnesium and Magnesium Alloys," *DMIC Memorandum 205*, June 1, 1965.
2. "Magnesium Finishing, Military Applications," Brochure, Dow Chemical Company, Metal Products Department.
3. "Products for Finishing Magnesium," Brochure, MacDermid Inc., Waterbury, Connecticut.
4. Stricklen, R., "A New Method of Protecting Magnesium," *Precision Metal Molding*, August 1954.

UNCLASSIFIED
CONFIDENTIAL

UNCLASSIFIED

IV. *Voyager* Project

A. Introduction

1. Objectives

The primary objective of the *Voyager* Program is to carry out scientific investigations of the solar system by instrumented, unmanned spacecraft which will fly by, orbit, and/or land on the planets. Emphasis will be placed on acquisition of scientific information relevant to the origin and evolution of the solar system; the origin, evolution, and nature of life; and the application of this information to an understanding of terrestrial life. The primary objective of the *Voyager* missions to Mars, beginning in 1973, is to obtain information relative to the existence and nature of extraterrestrial life; the atmospheric, surface, and body characteristics of Mars and the planetary environment by performing automated experiments on the surface of, and in orbit about, the planet. A secondary objective is to further our knowledge of the interplanetary medium between the planets Earth and Mars by obtaining scientific and engineering measurements while the spacecraft is in transit.

2. Project Plan

All *Voyager* missions will be conducted as events of an integrated program in which each individual flight forms a part of a logical sequence in an over-all technical plan of both lander and orbital operations. The *Voyager* design will provide for the carrying of large scientific payloads to the planet, the telemetering of a high volume of data back to Earth, and long useful lifetimes in orbit about the planet and/or on the planetary surface. Hardware will be designed to accommodate a variety of spacecraft and/or capsule science payloads, mission profiles, and trajectories. Particular emphasis will be given to simple and conservative designs, redundancy wherever appropriate, and a comprehensive program of component, subsystem, and system testing.

Over-all direction and evaluation of the *Voyager* Program is the responsibility of the Office of Space Science and Applications (OSSA) of the National Aeronautics and Space Administration (NASA).

An interim project management office consisting of OSSA personnel will be established at Pasadena, California, for *Voyager* Project management, supported by the Jet Propulsion Laboratory (JPL) of the California Institute of Technology in the mission analysis and engineering area. System responsibilities assigned to JPL are: surface laboratory system, tracking and data acquisition system, and mission operations system; assigned to Marshall Space Flight Center (MSFC) are *Saturn V* launch vehicle system and spacecraft system; and to Langley Research Center (LRC) the capsule bus system has been assigned.

UNCLASSIFIED

UNCLASSIFIED
CONFIDENTIAL

3. Technical Description

Planning shall be based upon launching two identical planetary vehicles by a single *Saturn V* launch vehicle at each Martian opportunity, starting with the 1973 opportunity. Each planetary vehicle is to consist of a flight spacecraft, flight capsule bus, and surface laboratory, with science experiments conducted in 1973 from the orbiter, during descent and on the planetary surface. The flight spacecraft with its capability for a 400-lb science subsystem (250 lb of instruments) will weigh approximately 2,500 lb; its retropropulsion subsystem may additionally weigh up to 15,000 lb; and the total flight capsule (capsule bus and surface laboratory) will weigh up to 5,000 lb. The flight spacecraft will be a fully attitude-stabilized device utilizing celestial references for the cruise phase, and will be capable of providing velocity increments for midcourse trajectory corrections and for Mars orbit attainment by both the flight spacecraft and the flight capsule. On-board sequencing and logic and ground command capability will be provided. The flight spacecraft will supply its own power from solar energy or from internal sources and will be capable of maintaining radio communications with Earth. In addition, the flight spacecraft will be thermally integrated and stabilized and will monitor various phenomena near Mars and during transit, and will telemeter this information back to Earth; it will monitor and telemeter data pertaining to spacecraft operations. The flight spacecraft will also provide the flight capsule with services such as power, timing and sequencing, telemetry, and command during the transit portion of the missions and may serve as a communications relay. The sterilized flight capsule bus will be designed for separation from the flight spacecraft in orbit, for attaining a Mars impact trajectory, for entry into the Martian atmosphere, for descent to the surface, and for soft-landing the surface laboratory, which will have surface lifetimes of up to 2 days in 1973 and later goals of as much as 6 mos. The flight capsule bus will contain the propulsion, guidance, control, communications, and data handling systems necessary to complete its mission, while the surface laboratory will contain all power, sequencing, and communications for the conduct of surface operations.

No deep-space flight tests of the flight spacecraft are planned, and compensation will be made by more extensive ground tests to the extent possible. The test program for the flight capsule, which is planned to include Earth-entry flight tests, will investigate entry dynamics.

During the capsule Phase B time period, assessment shall be made of the quantitative effect of various growth factors on useful landed weight including increases in launch vehicle performance, increase in minimum Martian surface pressure, and availability of current weight contingency.

4. Sequence of Events

The Project plan is being implemented as follows:

The Spacecraft System procurement activity (Task C) is continuing with the three Phase B fixed-price JPL contracts for the accomplishment of mission, system, and management studies. One system contractor will be selected, through competition, for award by MSFC of a CPAF Phase C contract and, subsequently, a multiple-incentive CPIF-type Phase D contract.

The procurement action for the total capsule system includes selection of multiple Phase B JPL contractors in the last quarter of FY 67 and subsequently, from among these, one Phase C and D LRC contractor for the capsule bus system will be selected to carry out Phases C and D of the capsule bus system procurement. The surface laboratory Phase C procurement will be open competition for one JPL contractor who will carry out Phases C and D.

B. Engineering Mechanics

1. Heat Shields for Out-of-Orbit Entry into Mars

Under the auspices of an informal Intercenter *Voyager* Heat Shield Coordination Group with representatives from Ames Research Center, Langley Research Center, and JPL, a preliminary investigation of the available materials for entry into the Martian atmosphere from orbit has been initiated. The first phase of this investigation, out-of-orbit ablation screening, is now complete. This phase consisted of a series of three test conditions (Table 1) simulating the expected Martian entry environment from out of orbit. The tests were made by R. Pope, Ames Research Center, on materials furnished by JPL.

Table 1. Test conditions for out-of-orbit ablation screening activity

Test condition	Cold wall heating rate, Btu/ft² sec	Stream enthalpy, Btu/lb	Pressure, atm	Total heating, Btu/ft²
1	15	1900	0.01	1500
2	30	3500	0.01	1500
3	50	6000	0.01	1500

UNCLASSIFIED
CONFIDENTIAL

UNCLASSIFIED

The test data on the 23 materials used are shown in Table 2. The back surface temperature and the mass of material lost were thought to be sufficient test information for this early screening activity. There were some side heating effects due to the small size of the models (1.25 in. in diameter), but these negative effects were similar for all tests and should not affect the relative performance of the various materials significantly.

Several fairly obvious conclusions can be drawn from Table 2. First, low density is desirable. The lower the density, the lower the thermal conductance, and, therefore, the better the insulation capacity. Second, the use of cork as a filler appears to provide the lowest composite conductance. Cork is the only material available which exists in the form of hollow polygons on the micro level. Third, sterilization is apparently somewhat beneficial since it drives out low molecular weight interstitially absorbed fluids, lessening the composite conductance by more than can be explained by weight loss alone. Fourth, foamed plastics without fillers may be an area with significant future application since foamed Teflon, which compares favorably with the more exotic composites, has one of the higher conductances of any pure plastic.

A plot of the temperature rise at the back surface versus density is shown in Fig. 1. For the out-of-orbit entry use, where the heating loads are small and where the insulation capability is the single most important concept, this figure is meaningful. The lowest value, regardless of density, represents, of course, the most efficient insulator. On the other hand, if more than one density of the same material is available, the two or more points show a trend which indicates the improvement in insulation capability which might be possible if homogeneous samples could be achieved in even lower densities. Every material has a minimum density into which it may be fabricated in a homogeneous form. This minimum is based on the limitations in the fabrication techniques used to form it into a sample.

Table 2. Preliminary results of ablation screening at Ames Research Center for *Voyager*–Mars out-of-orbit missions

Material	Density ρ, lb/ft^3	ρX, lb/ft^2	Temperature rise at back face, °K			Total mass loss, %		
			$q = 15$ Btu/ft^2 sec	$q = 30$ Btu/ft^2 sec	$q = 50$ Btu/ft^2 sec	$q = 15$ Btu/ft^2 sec	$q = 30$ Btu/ft^2 sec	$q = 50$ Btu/ft^2 sec
1. Armstrong cork 2755	31.2	2.0	41	32	31	11.33	12.35	11.72
	31.2	1.0	56	46	37	20.3	22.9	21.4
2. Armstrong cork 2755, sterilized	26.1	2.0	44	36	23	11.39	12.94	12.47
3. GE 1004AP	33.0	2.0	92	75	64	4.85	5.36	4.80
4. GE 1004AP, sterilized	30.5	2.0	69	61	52	3.98	5.07	4.69
5. GE 1004AP, low density	22.2	2.0	57	54	44	3.68	4.77	5.48
	22.2	1.0	137	135	111	4.6	8.6	9.8
6. Hughes phenolic nylon	36.0	2.0	80	56	42	9.33	10.70	10.93
7. Avco 5026-39 with HCG	33.3	2.0	77	56	49	9.92	10.50	9.82
8. Avco Mod 5 (purple blend)	42.4	2.0	81	72	62	6.78	7.67	6.67
	42.4	1.0	141	118	103	11.4	15.3	14.3
9. McDonnell B45 RF with HC	40.3	2.0	98	70	62	6.16	7.38	6.23
10. McDonnell B45 RF without HC	37.2	2.0	77	71	63	7.23	7.14	5.84
11. High density Teflon	137.0	2.0	240	176	141	10.65	20.58	18.46
12. Avco 5026-99	24.3	2.0	51	40	29	8.1	8.3	7.5
	24.3	1.0	86	71	55	13.5	17.6	16.8
13. Avco foamed Teflon	46.8	2.0	68	50	40	22.5	23.9	20.8
14. Avco foamed Teflon	33.7	2.0	49	37	30	25.2	24.8	22.1
15. Boeing polyborazole	34.9	2.0	52	41	42	11.1	12.3	21.1
16. Avco 5026-39	33.3	2.0	65	56	48	9.4	9.5	10.0
17. Avco Mod 7	42.4	2.0	87	69	64	7.6	8.1	7.8
18. Avco Mod 20	42.4	2.0	75	62	58	8.6	9.1	8.5
19. McDonnell B-46RF	36.5	2.0	83	64	52	5.9	6.0	6.3
20. McDonnell B-47RF	25.2	2.0	53	40	35	9.4	12.3	9.4
21. Avco high cork	28.3	2.0	47	32	28	9.1	10.4	10.0
22. Lockheed quartz fiber	15.5	1.0	79	58	52	0.6	0.6	1.1
23. Martin SLA-561	12.5	1.0	62	51	42	11.3	12.0	11.1

CONFIDENTIAL UNCLASSIFIED

UNCLASSIFIED
CONFIDENTIAL

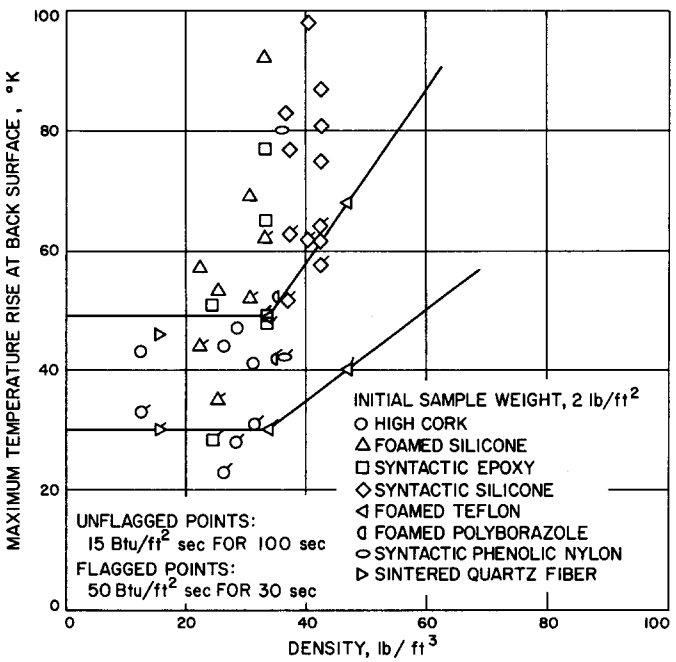

Fig. 1. Effect of density on the insulation capability of various candidate materials systems for out-of-orbit entry into Mars

An example is shown with the Teflon lines drawn on Fig. 1. For its density, foamed Teflon appears to be the most efficient material in the figure. The lowest density, though, is presently the lowest available using the given processing method. Hence, the flat extension of the line across the figure to the zero density line. Any material which is below this line for either heating rate, or which can be hypothesized to be below this line in those lower density versions which could be realistically assumed to be fabricable, is worth investigating further for the out-of-orbit entry mode. Those materials in the figure which meet these criteria are primarily materials high in cork (greater than 50%). A syntactic epoxy foam material, one variety of foamed silicone elastomer, foamed polyborazole, and perhaps the sintered quartz fiber are also somewhat competitive and warrant some further consideration as candidate materials for the out-of-orbit mode of entry into Mars.

Other activities presently in process as part of the cooperative efforts of this intercenter coordination group mentioned earlier, are: sterilization and transit environment screening, an investigation of ablation processes in the direct hyperbolic entry mode into Mars, and the relative RF transparency before and after ablation of the better heat shield materials from the above tests. The results of these activities will be reported as they become available.

2. Transistor Sterilization Test Program: 2000-hr Interim Report Summary

a. Introduction. The *Voyager* spacecraft are planned to fly by, orbit, and land on various planets to research the existence and origin, as well as the evolution and nature, of life beyond Earth. To accomplish this, it is necessary that these spacecraft be sterilized and decontaminated of all Earth-born microorganisms. Therefore, the spacecraft components must be subjected to sterilization heat cycles.

The present test program was designed to evaluate the effect of temperature sterilization on the reliability of 38 different silicon semiconductors (Table 3) representing the following transistor types: high frequency, signal, medium power, power, unijunction, chopper, field effect, and dual. The main purpose was to obtain sufficient part-type candidates for the JPL Sterilization Parts List (ZPP-2110-SPL). Also, valuable long-life reliability data were to be generated and analyzed. Begun January 28, 1965, it is scheduled for completion in February 1967.

3. Description of Tests

An outline of the test program is given in Fig. 2. For the tests, 100 units of each of the 38 semiconductor types were divided into the following three categories:

Group	Number of units	Tests
A	45	Environmental and 10,000-hr operating life tests; no temperature sterilization
C	45	Temperature sterilization; environmental and 10,000-hr operating life tests, followed by a 250-hr operating life test
D	10	Temperature sterilization; environmental and 10,000-hr temperature storage tests, followed by a 250-hr operating life test

UNCLASSIFIED
CONFIDENTIAL

UNCLASSIFIED

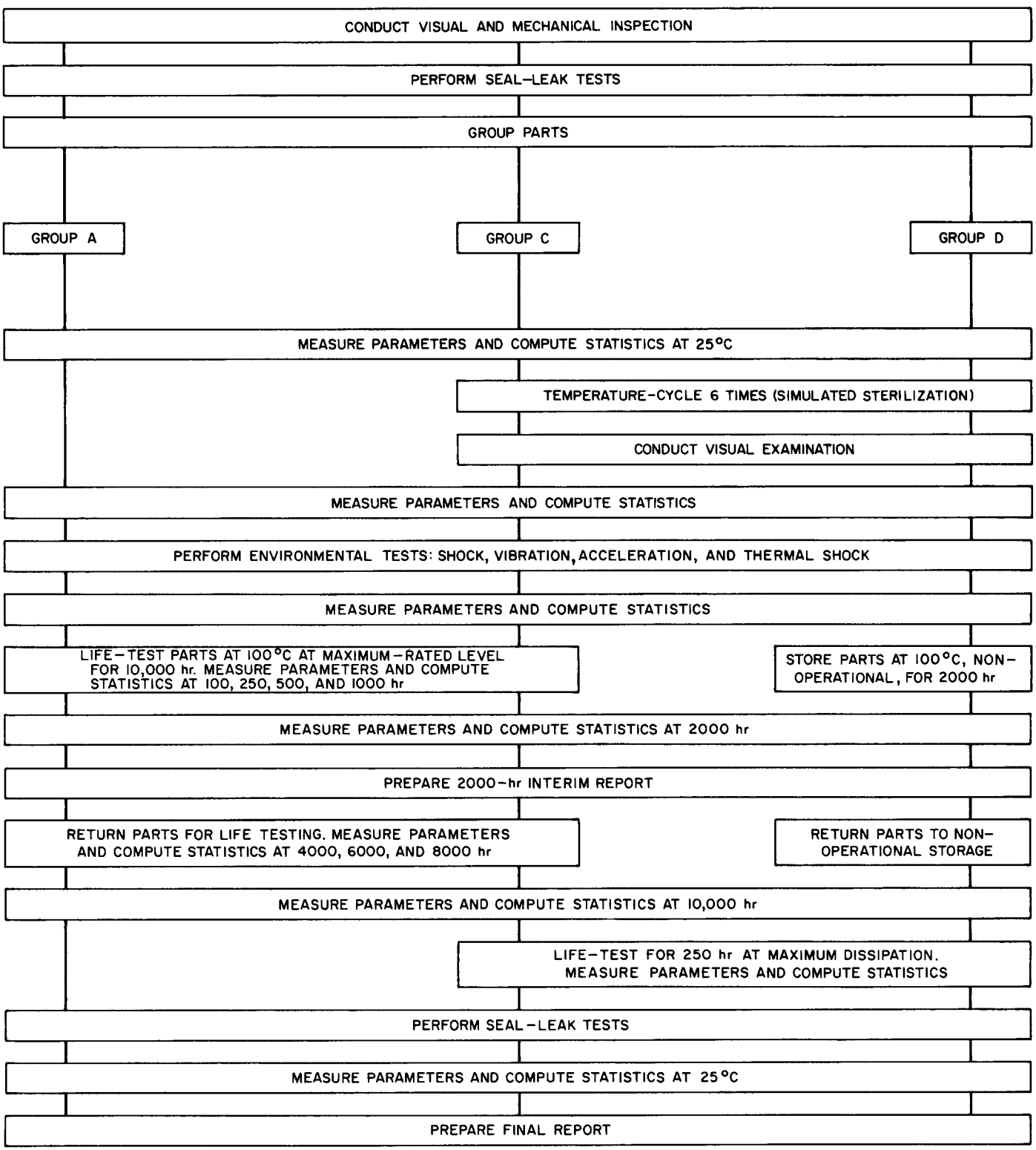
CONDUCT VISUAL AND MECHANICAL INSPECTION
PERFORM SEAL–LEAK TESTS
GROUP PARTS
GROUP A
GROUP C
GROUP D
MEASURE PARAMETERS AND COMPUTE STATISTICS AT 25°C
TEMPERATURE-CYCLE 6 TIMES (SIMULATED STERILIZATION)
CONDUCT VISUAL EXAMINATION
MEASURE PARAMETERS AND COMPUTE STATISTICS
PERFORM ENVIRONMENTAL TESTS: SHOCK, VIBRATION, ACCELERATION, AND THERMAL SHOCK
MEASURE PARAMETERS AND COMPUTE STATISTICS
LIFE–TEST PARTS AT 100°C AT MAXIMUM–RATED LEVEL FOR 10,000 hr. MEASURE PARAMETERS AND COMPUTE STATISTICS AT 100, 250, 500, AND 1000 hr
STORE PARTS AT 100°C, NON–OPERATIONAL, FOR 2000 hr
MEASURE PARAMETERS AND COMPUTE STATISTICS AT 2000 hr
PREPARE 2000–hr INTERIM REPORT
RETURN PARTS FOR LIFE TESTING. MEASURE PARAMETERS AND COMPUTE STATISTICS AT 4000, 6000, AND 8000 hr
RETURN PARTS TO NON–OPERATIONAL STORAGE
MEASURE PARAMETERS AND COMPUTE STATISTICS AT 10,000 hr
LIFE–TEST FOR 250 hr AT MAXIMUM DISSIPATION. MEASURE PARAMETERS AND COMPUTE STATISTICS
PERFORM SEAL–LEAK TESTS
MEASURE PARAMETERS AND COMPUTE STATISTICS AT 25°C
PREPARE FINAL REPORT

Fig. 2. Transistor sterilization test program flow chart

UNCLASSIFIED

Group B (3 sterilization cycles, as specified in ZPP-2100-Gen A) was deleted from the program to reduce the number of devices to be tested. The following environmental tests were conducted:

(1) *Heat sterilization:* Groups C and D were subjected to 6 cycles of 36 hr at 145°C, followed by 24 hr at 25°C.

(2) *Shock:* The transistors were subjected to 30 shock impacts, with each impact consisting of 1500 *g* for 0.5 msec, as applied in each of three mutually perpendicular planes (10 impacts/plane).

(3) *Vibration:* The transistors were subjected to 35-*g*-rms acceleration, swept sinusoidally from 70 to 3000 cps and returned to 70 cps during a 15-min period (with sweep rate proportional to frequency), with the transistors hard-mounted in each of three mutually perpendicular planes.

(4) *Acceleration:* The transistors were subjected to a constant acceleration of 20,000 *g* for 1 min and were so oriented that the acceleration vector was in the direction most likely to produce mechanical failure.

(5) *Thermal shock:* The transistors were subjected to thermal shock in accordance with Method 107A, Test Condition A, MIL-STD-202B.

All life tests are being conducted at 100°C and at the power levels given in Table 3.

Table 3. Silicon semiconductors tested

Manufacturer	Device type	Description	Operating life test power, mw
Fairchild Semiconductor	2N914	NPN high frequency	205
Fairchild Semiconductor	2N918	NPN high frequency	115
Fairchild Semiconductor	2N930	NPN signal	150
Texas Instruments Incorporated, Semiconductor-Components Div.	2N930	NPN signal	150
Fairchild Semiconductor	2N2369	NPN signal	205
Sperry Rand Corp., Sperry Semiconductor Div.	2N2605	PNP signal	230
Texas Instruments Incorporated, Semiconductor-Components Div.	2N2412	PNP signal	170
Fairchild Semiconductor	2N995	PNP signal	205
General Electric Co.	2N2243A	NPN signal	455
Texas Instruments Incorporated, Semiconductor-Components Div.	2N2243A	NPN signal	455
Fairchild Semiconductor	2N708	NPN medium power	205
Texas Instruments Incorporated, Semiconductor-Components Div.	2N708	NPN medium power	205
Fairchild Semiconductor	2N956	NPN medium power	275
Texas Instruments Incorporated, Semiconductor-Components Div.	2N956	NPN medium power	275
Fairchild Semiconductor	2N722	PNP medium power	200
Texas Instruments Incorporated, Semiconductor-Components Div.	2N722	PNP medium power	200
Fairchild Semiconductor	2N910	NPN medium power	300
Texas Instruments Incorporated, Semiconductor-Components Div.	2N910	NPN medium power	300
Motorola Semiconductor Products, Inc.	2N2222	NPN medium power	250
Texas Instruments Incorporated, Semiconductor-Components Div.	2N1937	NPN power	2000
Silicon Transistor Corp.	2N2034	NPN power	344
Texas Instruments Incorporated, Semiconductor-Components Div.	2N2150	NPN power	1000
General Electric Co.	2N491B	Unijunction	160
General Electric Co.	2N2647	Unijunction	75
Sperry Rand Corp., Sperry Semiconductor Div.	2N943	PNP chopper	125
Motorola Semiconductor Products, Inc.	2N2331	NPN chopper	250
Texas Instruments Incorporated, Semiconductor-Components Div.	2N2432	NPN chopper	150
Amelco, Inc.	FE200 (2N3066)	N channel field effect	60[a]
Texas Instruments Incorporated, Semiconductor-Components Div.	2N2497	P channel field effect	35[a]
Siliconix	2N2608	P channel field effect	50[a]
Fairchild Semiconductor	2N2060	NPN dual	170
Texas Instruments Incorporated, Semiconductor-Components Div.	2N2642	NPN dual	150
Motorola Semiconductor Products, Inc.	2N708	NPN medium power	205
Motorola Semiconductor Products, Inc.	2N722	PNP medium power	200
Motorola Semiconductor Products, Inc.	2N914	NPN high frequency	205
Motorola Semiconductor Products, Inc.	2N995	PNP signal	205
Motorola Semiconductor Products, Inc.	2N2369	NPN signal	205
Motorola Semiconductor Products, Inc.	2N2412	PNP signal	170

[a]Drain supply voltage, v.

4. Failure Analysis

Various statistical methods were employed to determine the effects of temperature sterilization upon the transistors. The significance of both the change in a group mean and the difference between the changes in different group means was tested using the *t*-statistic. The individual measurement variability between groups was tested using the *F*-statistic. Catastrophic and parametric failures between groups were tested using the Chi-square (χ^2) statistic. Outlier detection was employed to temporarily remove the measurement data of the outliers (approximately 4 standard deviations from the mean) from the statistical computations.

The catastrophic failures which occurred during the initial 2000 hr of the 10,000-hr operating life test can be attributed to randomness and were insufficient to provide statistical conclusions on the effects of sterilization. Analysis of these failures generally indicated poor workmanship, such as faulty bonding, defective oxide layers, cracked or chipped die, and contamination. The only predominant failure mode was the interaction of gold, silicon, aluminum, and heat ("purple plague"), which degraded the bonds and thereby caused a large number of bond failures. This problem is best resolved by using aluminum wire bonded to aluminum pads (a technique now in use by most manufacturers).

Statistical comparison of the number of parameter failures in Group A (not sterilized) versus those in Group C (sterilized) on an over-all basis revealed no significant difference between the two groups. However, a very significant difference was noted when these two groups subjected to operating life tests were compared on an over-all basis to Group D (sterilized), which was subjected to temperature storage. Group D had significantly fewer failures than either Group A or Group C. It can be concluded that, in some instances, life testing and repeated measurements degraded the devices.

The high incidence of parametric failures is alarming. During initial measurements, 196 of the 3800 devices involved failed to meet their own manufacturer's tolerances. Others were so close to being out-of-tolerance that, by the end of the 2000-hr measurement period, 731 had drifted out-of-tolerance and become parametric failures. This represents a parametric failure incidence of approximately 20%. The quality varied widely among the device types of all manufacturers. To evaluate the behavior of parametric failures during the 10,000-hr operating life test, no physical failure analysis will be performed until the end of the test program.

5. Summary of Results

The results obtained thus far may be summarized as follows:

(1) Heat sterilization at 145°C had no significant effect on the catastrophic or parametric failures during the 2000-hr measurement period.

(2) Power-applied versus storage groups displayed significantly more failures for the power-applied groups with several of the transistor types.

(3) A very high incidence of parametric failures occurred, which points out the need to use high-reliability parts for spacecraft hardware, including burn-in and environmental stress screens.

(4) The over-all difference in performance between the manufacturers was negligible.

(5) The only predominant catastrophic failure mode was purple plague, leading to junction-bond failures. Otherwise, generally poor workmanship was indicated by the failure analysis.

(6) The PNP devices incurred twice as many parametric failures as did the NPN devices. (There were insufficient high-power part types to make a comparison between these and the low-power types.)

(7) The predominant parametric-failure modes for the NPN and PNP devices was excessive junction leakage and degraded current gain during life testing.

CONFIDENTIAL UNCLASSIFIED

UNCLASSIFIED
CONFIDENTIAL

V. Future Projects

A. Introduction

The Future Projects Office of the Laboratory is responsible for the direction, sponsorship and, in cooperation with other elements of the Laboratory, the origination of advanced mission and future project studies in the areas of interest and applicability to the Laboratory.

The objective of this effort is to insure that the preliminary technical information and plans for the various potential missions, together with the associated information on spacecraft systems, instrumentation systems, launching vehicle systems, resources, and schedule be available as required. This preliminary mission study information will be used primarily for defining specific flight mission programs and as generalized guidance for the Laboratory research and advanced development programs.

Each study conducted by this Future Projects Office has been, and will continue to be, documented in a formal final report. This section of the Space Programs Summary is allocated to provide an abstract or summary of the results of each study including, where appropriate, reference to the final report for additional details.

B. Some Scientific Instruments for an Unmanned Lunar Orbiter[1]

a. Introduction. The Space Science Board of the National Academy of Sciences (Ref. 1) has defined three categories of basic problems concerning the Moon. These three categories have been further elaborated upon by defining a number of basic questions that should be answered in a total program of lunar exploration. The Space Science Board questions encompass virtually all problems of lunar research and should dictate the objectives of lunar exploration. Obviously, however, no one mission, manned or unmanned, can answer all of these basic scientific questions about the Moon; thus, the total program for lunar research must involve laboratory studies, as well as lunar impacters, orbiters, hard landers, soft landers, and manned missions.

The Office of Advanced Studies at the Jet Propulsion Laboratory has been asked by NASA Headquarters, Office of Lunar and Planetary Programs, to determine the most effective scientific manner in which all of the required objectives for lunar exploration can be accomplished, and

[1]From EPD-472, "Scientific Instruments For Lunar Exploration," Part A, Lunar Orbiter Unmanned, JPL, January 1967.

UNCLASSIFIED
CONFIDENTIAL

UNCLASSIFIED

to derive a total lunar exploration program in terms of a mix of specific projects and missions. One part of the above task involves the derivation of an extended list of scientific instruments and objectives. The purpose of this report is to define such a list for an unmanned lunar orbiter spacecraft.

b. Mission constraints. The lunar orbiter spacecraft is ideally suited for a reconnaissance mission and for obsering those parameters of the lunar environment that are subject to temporal or spatial change. A great deal of the environmental information that is desirable to know about the Moon, both from the point of view of answering the Space Science Board questions and providing data for future missions, is synoptic in nature; therefore the number of scientific experiments that can be accomplished on a mission of this type needs to be limited by some selection process. For this report, the following constraints are imposed:

(1) Those scientific experiments that can be done as well on terrestrial orbiters or other space missions are excluded from consideration here; however, several experiments to characterize the energetic radiation near the Moon, with particular emphasis on determining the long-term radiation hazards to manned lunar flights, have been included.

(2) The primary mission of the lunar orbiter is reconnaissance and correlation; thus, it should not be considered, generally, as a tool for acquiring absolute data on the physical and chemical properties of the lunar surface at a specific point, but rather as a mode for measuring or detecting variations in a particular property of the Moon with change of surface location.

(3) The time period for this mission is up to, and including, 1973; thus, long lead-time development items are not considered as practical, and instrument availability is limited by current engineering knowledge and state-of-the-art.

(4) No effort has been made to order or assign priorities to the scientific instruments either in terms of Space Science Board questions, or recommendations by the Manned Space Science Coordinating Committee (Ref. 2); however, the scientific objectives for each experiment discussed in the text are given.

The requirements of the instruments impose a burden on the design of the vehicle. For example, the attitude control system should not contaminate the measurements of such items as particle density, atmospheric pressure, and composition. For the same reason, care must be used whenever pressurized containers are employed to prevent leakage, and considerations should be given to the outgassing of the vehicle. Outgassing of the vehicle should occur fairly rapidly in space; however, it may be prolific enough to make a delay of instrument operation desirable until it has taken place. In addition, the possible effect on scientific instruments from any onboard radiation source, such as an RTG unit, must not be overlooked.

Placement of the instruments is extremely important. If sensitive magnetometers are used, they must be placed at a sufficient distance from the magnetic materials and electronic components. The wires leading to and from the instrument must be carefully considered. A single turn of wire carrying 10 μa produces a field of 1 gamma. This exceeds the error capability of some magnetometers. Instruments used for observing electromagnetic or corpuscular radiation must be placed so as to minimize the effects of secondary radiation or shielding by the vehicle itself. In addition, care must be taken so as not to introduce errors due to the cosmic albedo of the Earth, if the instruments are pointed toward the Earth.

Similar problems exist with such instruments as ionization gauges and mass spectrometers. Since the velocity of the vehicle is comparable with the velocity of gas molecules and the free mean paths of these particles are in the order of meters, the satellite tunnels out a rather severe vacuum in its wake. Thus, the instrument will not operate properly if its opening is rear-facing. In addition, the openings of this type of instrument must be carefully considered to prevent an enforced separation of gases according to mass. Because of the large mean free paths, the lighter gases enter more quickly than the heavier ones.

Erosion of the outer surface by micrometeorites and radiation may affect the scientific instruments. Sputtering of metal caused by collision with ambient ions or neutral particles can be serious, especially for spacecraft that are expected to perform their mission over an extended period of time, e.g., more than 30 days. Experience gained from the present series of lunar orbiters will be very valuable in solving problems relating to the choice of second generation missions and experiments.

Finally, very special consideration will have to be given to the design of a telemetry link for communications between the lunar orbiter and the Earth. The data rate will be very high if all of the suggested experiments are to be accommodated; thus, some type of onboard data compression technique, either by selection or integration, will

CONFIDENTIAL UNCLASSIFIED

UNCLASSIFIED
CONFIDENTIAL

be required. Also, the requirements for an adequate buffer or storage device to hold lunar backside information until it can be transmitted should be noted. It appears that the lunar orbiter mission will not be particularly limited by weight and power, nor by the state-of-the-art in sensor or instrument design, but limited rather by the data capacity of the communication link.

c. Instruments or experiments. A "shopping list" of representative lunar scientific instruments that can be used on an unmanned lunar orbiter spacecraft is presented in Table 1. It should be noted that virtually all of the experiments considered for terrestrial orbiters, such as the geophysical satellite series and various atmospheric probes, could have an application to lunar orbiter science. Thus, in the case for a lunar atmospheric experiment, only the mass spectrometer has been considered in this report; however, the Langmuir Probe, for measuring the electron temperature and density, and the Redhead Gage, for directly measuring the atmospheric pressure, are also feasible scientific instruments for a lunar orbiter mission; there are obviously many others. The list of experiments discussed here is certainly not complete; however, it is considered typical and appropriate, under the constraints defined above, for providing the kind of information that is required for mission study purposes.

As stated earlier, many of the experiments that have been considered for terrestrial orbiters and atmospheric probes could have an application to lunar orbiter science. In addition to these, however, there are several categories of experiments that, while not discussed in the foregoing table, should at least be kept in mind by any group that is considering the question of the types of experiments that can be accomplished on a lunar orbiter mission. Some of these are:

Radio transmission. A radio transmission experiment (either orbiter-to-surface or orbiter-to-Earth) with wavelengths of the order of tens of meters or greater should be considered in order to investigate the conductivity or dielectric constant of deeper layers of the Moon.

Gamma ray or x-ray telescope. A gamma ray or x-ray telescope in an appropriate lunar orbit should be useful for studying the occultation of many more cosmic sources than can be done from Earth. The objective of occultation experiments is to make accurate determinations of the angular size of such sources.

UV instruments. An entire class of UV instruments may be of importance. Although little is presently known about it, fluorescence in this wavelength region may be useful in detecting the collapse of a lunar bow shock against the surface, which might result from an increase in solar wind pressure. Also, UV imaging and UV spectroscopy of selected areas could become rather high priority experiments.

Table 1. Select list of lunar orbiter science

Instrument or experiment	Weight, lb	Power, w	Data rate, bits/sec	Scientific objectives
1. Helium magnetometer	5	4	1 bit/sec minimum (sample every 30 sec) 100 bit/sec desired	1. Map any lunar magnetic field and determine its magnitude, orientation and characteristics. 2. Study the flow past the Moon of the solar plasma with its embedded magnetic field.
2. Search coil magnetometer	5	2	1 bit/sec minimum (sample every 30 sec) 100 bit/sec desired	Investigate the hydromagnetic flow of the solar plasma around the Moon and the nature of any interface region.
3. Plasma detector	15	10	50	1. To determine the low-energy charged-particle environment of the Moon. 2. To aid in the interpretation of the magnetometer data by a study of the interaction of the Moon with the solar plasma and magnetic field.
4. Meteor dust detector	7	1	1	To measure the velocity, mass and distribution of dust particles in the vicinity of the Moon.

UNCLASSIFIED
CONFIDENTIAL

UNCLASSIFIED

Table 1 (contd)

Instrument or experiment	Weight, lb	Power, w	Data rate, bits/sec	Scientific objectives
5. Body properties	N/A	N/A	N/A	To determine the mass, the mean moment of inertia, and the coefficients in the expansion for the gravitational potential of the Moon.
6. Radar	50	22	See text	To provide information about the spacecraft altitude and properties of the lunar surface, such as surface roughness, reflectivity, dielectric properties, etc.
7. Gamma-ray spectrometer	25	4	500	To determine the approximate concentration of radioactive materials present in the lunar surface.
8. Thermal neutrons detector	8	2	50	To measure the energy spectrum of albedo neutrons to determine an approximate value for the concentration of hydrogen in the lunar crust.
9. Thermal mapping	25–60	55	660	To map the temperature of the lunar surface and its emissivity as a function of position and phase angle. See also infrared mapping in text.
10. X-ray fluorescence	18	2	500	To measure the approximate relative abundance of iron and nickel in the material making up the top of the lunar surface.
11. Microwave surface imager	35	15	250	To measure the three-dimensional temperature distribution of the Moon's crust.
12. Photo-imaging experiment	25 for indexing camera; 150 for stereo system	10–30	10^3	To provide basic data on lunar geology as well as information for preparing a base map that will be used to collate the data from the other experiments.
13. Quadrupole mass spectrometer	12	10	250	To measure neutral mass spectrum, neutral particle pressure, total ion concentration, directed ion flux, and ion mass spectrum.
14. Tissue-equivalent dosimeter	1	2 mw	5	To provide data on the biological hazards due to energetic radiation resulting from prolonged stays in the vicinity of the Moon.

References

1. Space Research, *Directions for the Future*, (1965), Part I, Space Science Board, National Academy of Sciences, National Research Council, Washington, D. C.
2. NASA, 1965 Summer Conference on Lunar Exploration and Science (1965), NASA *SP-88*, National Aeronautics and Space Administration, Washington, D. C.

CONFIDENTIAL UNCLASSIFIED